



JGR Atmospheres

RESEARCH ARTICLE

10.1029/2024JD040743

Special Collection:

Emerging air pollution: emissions, chemistry, and health and climate effects

Key Points:

- Volatile chemical product emissions accounted for 23% of mean daily max 8-hr ozone in ozone episodes, as per the 2010 CalNex study
- VCP emissions boost ozone formation by increasing primary production and efficient recycling of ROx radicals, thus enhancing pollution
- 2020s reduction in NOx emissions in Los Angeles, potentially due to COVID-19, led to a NOx-limited state, lessening VCPs' impact on ozone

Supporting Information:

Supporting Information may be found in the online version of this article.

Correspondence to:

J. de Gouw and L. Xue, joost.degouw@colorado.edu; xuelikun@sdu.edu.cn

Citation:

Chen, T., Gilman, J., Kim, S.-W., Lefer, B., Washenfelder, R., Young, C. J., et al. (2024). Modeling the impacts of volatile chemical product emissions on atmospheric photochemistry and ozone formation in Los Angeles. *Journal of Geophysical Research: Atmospheres*, 129, e2024JD040743. https://doi.org/10.1029/2024JD040743

Received 5 JAN 2024 Accepted 10 MAY 2024

Modeling the Impacts of Volatile Chemical Product Emissions on Atmospheric Photochemistry and Ozone Formation in Los Angeles

Tianshu Chen^{1,2} , Jessica Gilman³ , Si-Wan Kim⁴ , Barry Lefer⁵ , Rebecca Washenfelder¹, Cora J. Young⁶ , Bernhard Rappenglueck^{7,8}, Philip S. Stevens^{9,10} , Patrick R. Veres¹¹, Likun Xue² , and Joost de Gouw^{1,12}

¹Cooperative Institute for Research in Environmental Sciences, University of Colorado Boulder, Boulder, CO, USA, ²Environment Research Institute, Shandong University, Qingdao, China, ³Chemical Sciences Laboratory, National Oceanic and Atmospheric Administration, Boulder, CO, USA, ⁴Department of Atmospheric Sciences, Yonsei University, Seoul, Korea, ⁵Division of Tropospheric Composition, National Aeronautics and Space Administration, Washington, DC, USA, ⁶Department of Chemistry, York University, Toronto, ON, Canada, ⁷Department of Earth and Atmospheric Sciences, University of Houston, Houston, TX, USA, ⁸Institute for Climate and Atmospheric Science, University of Houston, Houston, TX, USA, ⁹O'Neill School of Public and Environmental Affairs, Indiana University, Bloomington, IN, USA, ¹⁰Department of Chemistry, Indiana University, Bloomington, IN, USA, ¹¹NSF National Center for Atmospheric Research, Boulder, CO, USA, ¹²Department of Chemistry, University of Colorado, Boulder, CO, USA

Abstract The dominant fraction of anthropogenic volatile organic compound (VOC) emissions shifted from transportation fuels to volatile chemical products (VCP) in Los Angeles (LA) in 2010. This shift in VOC composition raises the question about the importance of VCP emissions for ozone (O₃) formation. In this study, O₃ chemistry during the CalNex 2010 was modeled using the Master Chemical Mechanism (MCM) version 3.3.1 and a detailed representation of VCP emissions based on measurements combined with inventory estimates. The model calculations indicate that VCP emissions contributed to 23% of the mean daily maximum 8-hr average O₃ (DMA8 O₃) during the O₃ episodes. The simulated OH reactivity, including the contribution from VCP emissions, aligns with observations. Additionally, this framework was employed using four lumped mechanisms with simplified representations of emissions and chemistry. RACM2-VCP showed the closest agreement with MCM, with a slight 4% increase in average DMA8 O_3 (65 \pm 13 ppb), whereas RACM2 $(58 \pm 13 \text{ ppb})$ and SAPRC07B $(59 \pm 14 \text{ ppb})$ exhibited slightly lower levels. CB6r2, however, recorded reduced concentrations (37 \pm 10 ppb). Although emissions of O₃ precursors have declined in LA since 2010, O₃ levels have not decreased significantly. Model results ascribed this trend to the rapid reduction in NO_X emissions. Moreover, given the impact of COVID-19, an analysis of 2020 reveals a shift to a NO_X-limited O₃ formation regime in LA, thereby diminishing the influence of VCPs. This study provides new insights into the impact of VCP emissions on O₃ pollution from an in-depth photochemical perspective.

Plain Language Summary In the 2010 CalNex study, researchers found that volatile organic compounds (VOCs) were predominantly emitted from volatile chemical products (VCPs) like solvents. In our subsequent research, using a detailed chemical model, we discovered that about a quarter of the mean daily maximum 8-hr average ozone was contributed by these everyday products during ozone episodes. This insight is critical as it underscores how these emissions significantly speed up ozone formation through accelerated chemical reactions. We also evaluated various simplified chemical mechanisms for ozone prediction, finding that the one incorporating key reactions of VOC species was most accurate. Further, our analysis suggests that the slight increase in Los Angeles' ozone levels since 2010 can likely be attributed to faster reductions in NO_X emissions relative to VOCs. Notably, the reduction in NO_X emissions by 2020 considerably diminished the impact of VCPs on ozone levels. However, given the uncertain future of NO_X emissions and the ongoing rise in emissions from everyday products, it remains essential to control these emissions.

1. Introduction

Ozone (O_3) is formed in the troposphere through photochemical reactions of volatile organic compounds (VOCs) and nitrogen oxides $(NO_X = NO + NO_2)$, and is a significant ground-level air pollutant with detrimental effects on human health and vegetation (Wang et al., 2022; Zhang et al., 2019). The rapid decrease in transportation-

© 2024. American Geophysical Union. All Rights Reserved.

CHEN ET AL. 1 of 19

related VOC emissions has increased the relative importance of other sources of VOCs, including volatile chemical product (VCP), which have emerged as the largest petrochemical source of urban organic emissions in the United States (US) (McDonald et al., 2018). VCPs, encompassing pesticides, coatings, printing inks, adhesives, cleaning agents, and personal care products, contain highly reactive VOCs, including organic solvents (McDonald et al., 2018). Laboratory studies have also demonstrated the impacts of VCPs on the aerosol formation (D. Lu et al., 2019; Shah et al., 2020; Wu & Johnston, 2017).

Assessment of VCP emissions and their contributions to atmospheric chemistry can be conducted through "topdown" (measurement-based) or "bottom-up" (emission inventory-based) analyses. A challenge for the "topdown" approach is the difficulty in measuring highly reactive VCP-emitted VOCs, for example, oxygenated VOCs (OVOCs) (de Gouw, 2021; McDonald et al., 2018). However, measurements of VCP species do help inform our understanding of overall VOC emissions in recent years. Coggon et al. (2021) found that VCPs are widespread in US and European cities by tracking the distribution of D5-siloxane. Gkatzelis et al. (2021) conducted VOC observations in two US cities with different population densities (Boulder and New York City), and found that VCP emissions accounted for 42% and 78% of anthropogenic VOC emissions, respectively. Gkatzelis et al. (2021) also identified ethanol, propylene glycol, ethylene glycol, dipropylene glycol, diethylene glycol, and monoterpenes as the dominant VCP species for OH radical loss (R_{OH}). These studies underscore the contribution of VCPs to urban VOC emissions and R_{OH} by field observations. The other approach involves using "bottom-up" methods. McDonald et al. (2018) constructed a VCP emission inventory using mass balance, and found that VCP emissions (7.6 \pm 1.5 Tg) are twice as high as those from mobile sources (3.5 \pm 1.1 Tg). Coggon et al. (2021) proposed an inventory (FIVE-VCP) that combined the fuel-based inventory of vehicle emissions with the VCP emissions inventory. Seltzer, Pennington et al. (2021) developed a framework called 'VCPy' to model VCP emissions in the US. These studies have advanced the scientific understanding of VCP emissions in the US.

Several studies have attempted to quantify the impact of VCP on O_3 using regional chemistry transport models (CTM). Seltzer, Murphy et al. (2021) employed the Carbon Bond chemical mechanism version 6r3, with updated relevant chemical components, and indicated that VCP contributed 1.5–5.8 ppb of daily maximum 8-hr average (DMA8) O_3 concentrations on average during summertime in major urban areas. Zhu et al. (2019) utilized the SAPRC-07 chemical mechanism and found that VCP contributed 17.4 ppb of simulated DMA8 O_3 concentration in the summer in California. Qin et al. (2021) increased the VCP emissions in the NEI 2011 by a factor of 3 as input for their CTM, finding that VCP emissions accounted for nearly 17% of the DMA8 O_3 (9 \pm 2 ppb) during summer in Los Angeles (LA). Coggon et al. (2021) employed the FIVE-VCP inventory in conjunction with the RACM-ESRL-VCP mechanism to simulate O_3 concentrations during heatwave events in New York City. RACM-ESRL-VCP is a modified chemical mechanism that includes chemistry of critical oxygenated VCP species. The simulation results showed that VCP contributes more than 10 ppb of DMA8 O_3 during heatwave events (Coggon et al., 2021). These studies have expanded our understanding of the impact of VCP emissions on O_3 pollution. However, many CTM simulations are limited by available observational constraints. Furthermore, the ability of lumped chemical mechanisms to reproduce the VCP chemistry has not been compared with that of a near-explicit mechanism.

Los Angeles (LA) has experienced photochemical pollution since the 1950s, due to its population density, fossil fuel emissions, special topography, and climatic conditions (South Coast Air Quality Management District, 1997). Consequently, this city has been a focal point for air pollution control in the US. Decades of research have explored diverse factors (meteorology, emissions, photochemistry) influencing LA's air pollution (Pusede & Cohen, 2012; Warneke et al., 2012). Despite improved air quality, LA's O_3 levels still exceed standards, with a notable rise since 2010 (Kim et al., 2022). This increase is attributed to shifts in the O_3 formation regime, NO_X lifetime changes (Laughner & Cohen, 2019), decelerating NO_X emission reductions (Jiang et al., 2018), and climatic factors like drought (Demetillo et al., 2019; Nussbaumer & Cohen, 2020). O_3 formation mainly depends on VOCs and NO_X interactions, with recent focus shifting to VCP emissions due to significant reductions in NO_X and VOCs from traditional sources (Warneke et al., 2012). However, their emissions are not fully constrained by measurements. Moreover, the commonly utilized lumped chemistry mechanisms were initially designed for hydrocarbon-rich VOC emissions and may not fully capture the chemistry of VCPs, which are rich in oxygenated VOCs (Goliff et al., 2013; Ruiz & Yarwood, 2013; Zong et al., 2018). Consequently, it is of practical importance to investigate the chemistry and inter-annual trends of O_3 and to explore potential control strategies amidst the transition of primary VOC sources in LA.

CHEN ET AL. 2 of 19

This study examines the contributions of VCP emissions to O_3 chemistry in LA, using intensive field observations, emission inventories, and detailed chemical box modeling. We investigate the O_3 chemistry, identifying the key processes for O_3 production, and quantify the contribution from VCPs during the CalNex-2010. We also assess the representation of VCP in O_3 chemistry across different lumped chemical mechanisms. Furthermore, we evaluate the model by examining O_3 inter-annual trends in LA from 2010 to 2020, and delineate the O_3 variation with the reduction of precursors and discuss potential emission control strategies for 2020s.

2. Methods

2.1. Research Area, Data, and Period

Los Angeles is situated in the South Coast Air Basin, encircled by mountains. The transport of air pollutants into and out of the basin is determined by factors such as heating, sea breezes, and topography-driven winds (Lu & Turco, 1994). The interplay of these factors frequently causes air masses to circulate back and forth during a typical summer day (R. Lu & Turco, 1994). Consequently, air masses can become trapped within the mountainous coastal region for several days, allowing for extensive photochemical processing and formation of secondary pollutants.

The CalNex 2010 was conducted at the California Institute of Technology campus in Pasadena during 15 May through 15 June 2010 (Figure 1). In this study, we focus on measurements taken from 2 to 8 June as our base case. The selected days meet three conditions: clear and cloud-free conditions, direct transport from the LA coast to Pasadena, and strong O_3 formation. A detailed explanation of why this period was selected can be found in Washenfelder (2011). From evening to 9 a.m., winds were very light and the site was mainly influenced by local emissions. In the afternoon, the propagation of sea breeze transported air masses from Downtown LA to Pasadena.

2.2. Box Model Tool, Mechanisms, and Evaluation

To investigate O₃ chemistry in Pasadena, the Framework for 0-D Atmospheric Modeling (F0AM) (Wolfe et al., 2016) was used. This framework allows for the implementation of various chemical mechanisms. In this study, the Master Chemical Mechanism (MCM) v3.3.1 was utilized to explore detailed chemical processes in the base case. MCM is a near-explicit mechanism that represents the degradation of 143 primary VOCs, including the major VCP species, integrated with the IUPAC inorganic nomenclature (Jenkin et al., 2003; Saunders et al., 2003). Lumped mechanisms such as SAPRC, Carbon Bond (CB), and the Regional Atmospheric Chemistry Mechanism (RACM) are usually used in CTMs. In this study, these mechanisms were compared with MCM to evaluate the representation of VCP species for O₃ chemistry. The SAPRC Mechanism Version 07B (SAPRC07B) was adopted in this study (Cai et al., 2011; Carter, 2010), as well as the Carbon Bond version 6r2 (CB6r2) (Ruiz & Yarwood, 2013; Yarwood et al., 2010). Additionally, two versions of RACM were utilized: RACM version 2 (RACM2) (Goliff et al., 2013) and RACM2-VCP. RACM2-VCP (or RACM-ESRL-VCP) is developed by Coggon et al. (2021) and adds propylene glycol, isopropanol and glycerol to the basic version of RACM2. It also updates the reaction mechanisms of ethanol, methanol, acetone, and ethylene glycol. To quantitatively assess the model performance, the index of agreement (IOA) parameter was employed, which is a measure of the agreement between simulated and observed concentrations of species (Y. Wang et al., 2017). The IOA ranges from 0 to 1, with higher values indicating better agreement. The IOA is determined as Equation 1:

IOA = 1 -
$$\frac{\sum_{i=1}^{n} (O_i - S_i)^2}{\sum_{i=1}^{n} (|O_i - \overline{O}| + |S_i - \overline{O}|)^2}$$
 (1)

where \overline{O} denotes the average observed concentration, O_i represents the observed concentration for each individual sample, and S_i signifies the simulated concentration, all measured in units of ppb. The subscript 'i' refers to the index corresponding to each sample. VOC including acetaldehyde concentrations were determined using a two-channel in situ gas chromatography-mass spectrometry instrument (Gilman et al., 2010). Formaldehyde was measured with a Hantzsch monitor (Rappenglück et al., 2010; Warneke et al., 2011), and glyoxal was quantified using broadband cavity-enhanced absorption spectroscopy (Washenfelder et al., 2011). The laser-induced

CHEN ET AL. 3 of 19

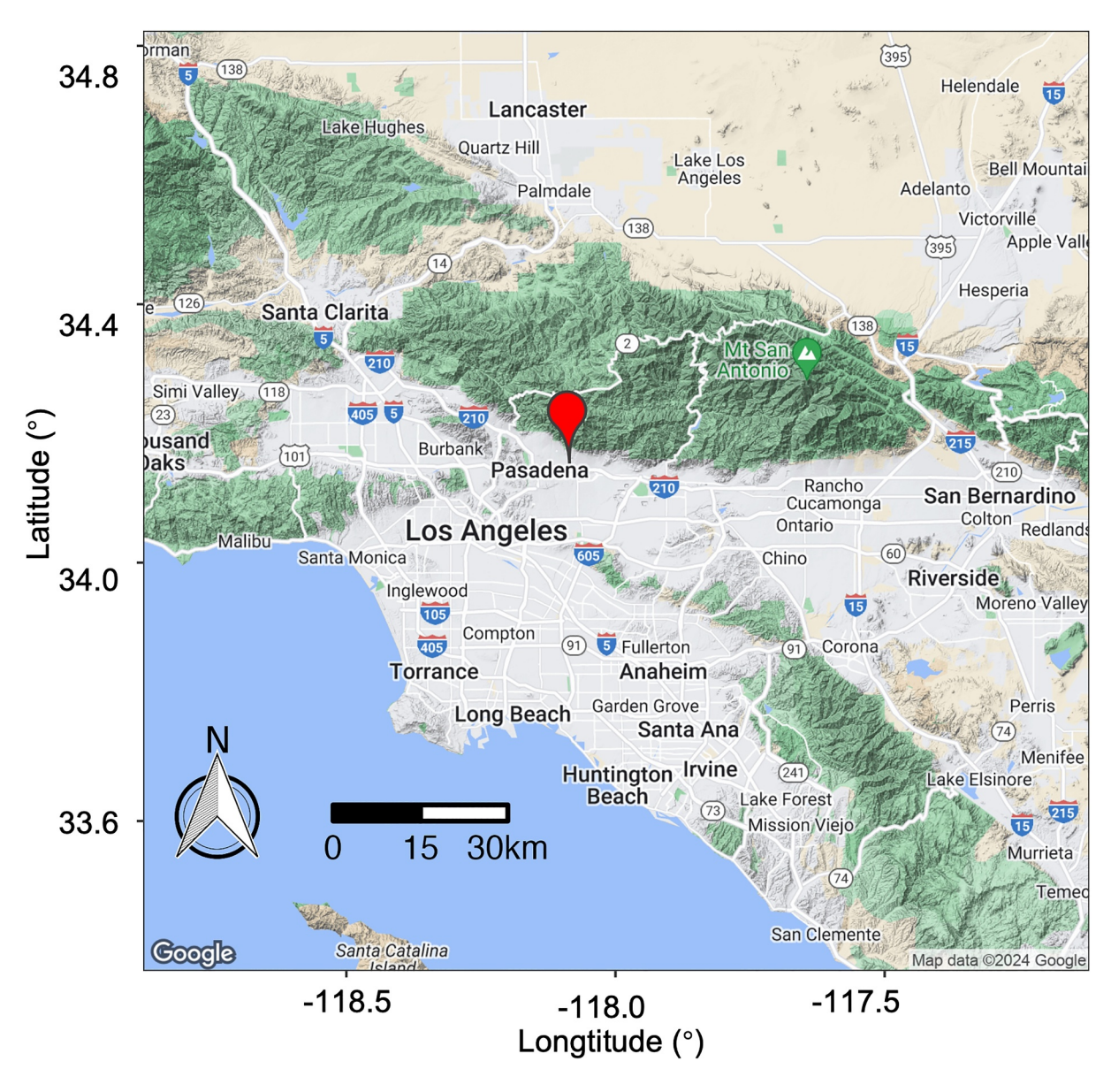


Figure 1. Los Angeles and location of the Pasadena ground site.

fluorescence-fluorescence assay by gas expansion technique was employed for Hydroxyl (OH) and hydroperoxy (HO_2) radicals measurement (Griffith et al., 2016). To aid in model comparison, all data were averaged over 30-min intervals.

2.3. Emission Rates During CalNex-2010

In the model, emissions of carbon monoxide (CO), NO_X , and VOCs are represented through a combination of emission inventories and measurement data. In the base case, CO and NO_X emission rates for Pasadena were obtained from a fuel-based inventory (S.-W. Kim et al., 2016) as was done in previous analyses (de Gouw et al., 2017). Emissions of CO and NO_X depended on the day of the week, with different emissions for (a) Monday through Thursday, (b) Friday, (c) Saturday, and (d) Sunday (refer to Figure S1 in Supporting Information S1). VOC emission rates were calculated by multiplying the CO emission rate with the emission ratio (ER) relative to CO reported elsewhere. Two types of emissions ratios were considered: observed emission ratios reported by de Gouw et al. (2017, 2018) based on VOC and CO data from CalNex 2010, and emission ratios for unmeasured VCP species, calculated according to the VCP emission inventory proposed by McDonald et al. (2018):

CHEN ET AL. 4 of 19

21698996, 2024, 11, Downloaded from https://agupubs.onlinelibrary.wiley.com/doi/10.1029/2024ID040743 by University Of Colorado Libraries

, Wiley Online Library on [03/06/2024]. See the

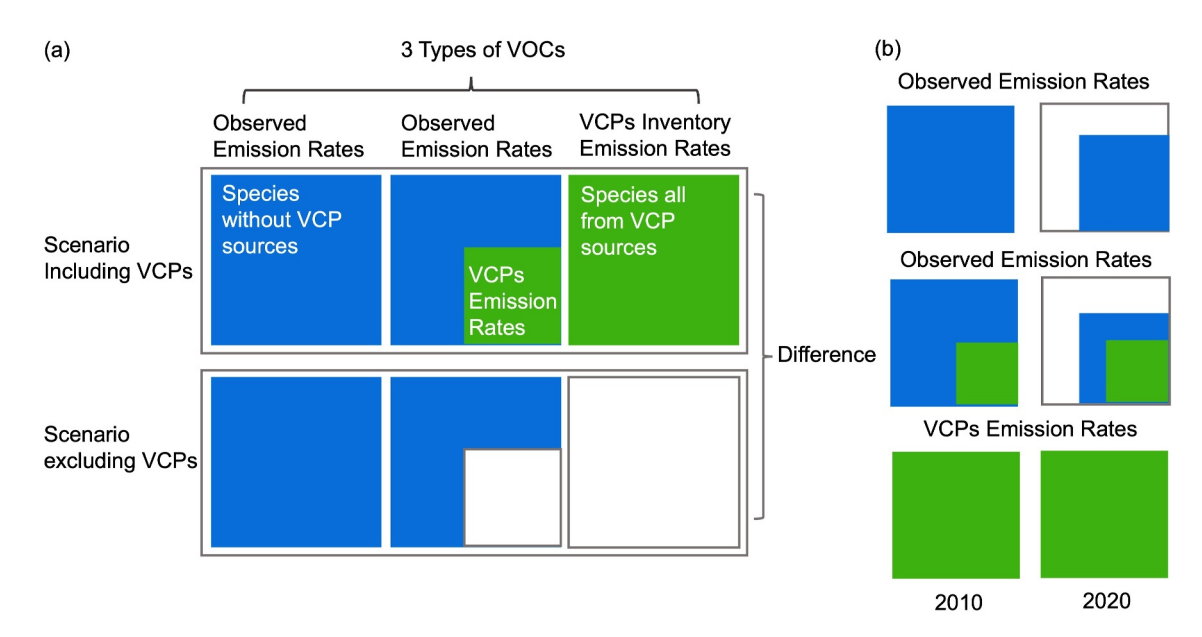


Figure 2. Concept figures for types of VOC and emission scenarios for (a) the base case and (b) inter-annual trends. Each square box represents VOC emissions. Blue indicates VOC emissions from non-VCP sources, while green signifies VOC emissions from VCP sources. In panel (a), the three columns represent three types of VOCs: those with no VCP sources, those partly from VCP emissions, and those entirely from VCP emissions. The two rows correspond to two different scenarios, with the blank section in the second row denoting the removal of VCP emissions in Scenario Two. In panel (b), the three rows correspond to the aforementioned VOC types, while the two columns represent scenarios for the years 2010 and 2020. The white sections illustrate the reduction in non-VCP source emissions from 2010 to 2020.

$$ER = \frac{\text{Annual Emission Amount of VCP in LA * Species Weight Percentage}}{\text{Annual Emission Amount of CO in LA}}$$
 (2)

The annual emission amount for each species is expressed in gigagrams (Gg). These values are then converted to moles using their respective molecular weights. Consequently, VOC species were classified into three types (Figure 2a).

- 1. VOCs that do not have VCP sources: emission ratios were determined using CalNex data.
- 2. VOCs measured during CalNex 2010 that do have VCP sources: emission ratios were determined using CalNex data, and the VCP-emitted contributions were calculated using Equation 2.
- 3. VOCs not measured during CalNex 2010 but known to have VCP sources: emission ratios were calculated with Equation 2.

VOC emissions were aggregated into different mechanisms for model input (Table S1 in Supporting Information S1). Species that are not included in MCM were substituted by MCM species exhibiting similar K_{OH} (Table S1 in Supporting Information S1).

2.4. Setup of Box Model

In the base case, CO, VOCs, and NO_X were emitted into the model at rates described in Section 2.3. A few comments should be made here.

- Biogenic VOCs are not emitted in proportion to CO; instead, isoprene, alpha-pinene, and beta-pinene were constrained by the observed concentrations. However, the observations were reduced by a factor of six to constrain the model, because, without that correction, the modeled products largely produced from biogenic VOCs (i.e., formaldehyde, methyl vinyl ketone, and methacrolein) significantly exceeded the measured values. This suggests that the measurements may be biased in terms of biogenic emissions, likely due to the close proximity of trees to the sampling inlet. The sensitivity of our conclusions for the factor of six reductions in biogenic VOCs will be discussed below.
- Limonene was emitted into the model as dictated by the VCP emission inventory, resulting in a higher modeled mixing ratio (0.04 ± 0.05 ppb) than observed (0.02 ± 0.01 ppb).

CHEN ET AL. 5 of 19

 NO_X emissions were specified as 80% nitric oxide (NO), 10% nitrogen dioxide (NO₂), and 10% HONO. It is important to note that 10% of the NO_X concentration was allocated to HONO emission to achieve a relatively reasonable HONO concentration (refer to Figure S2 in Supporting Information S1 for a comparison between the modeled and measured HONO concentrations).

Physical loss was constrained by dry deposition and dilution (including morning intrusions of free tropospheric O_3). Dry deposition of various peroxy acetyl nitrates (PANs), peroxides, inorganic gases, acids, and carbonyls was represented in the model following Zhang et al. (2003). In accordance with previous work by Edwards et al. (2014) and Wolfe et al. (2016), a first-order loss parameter (k_d) with background concentration was utilized for all species to represent all physical loss other than dry deposition:

$$\frac{\mathrm{d}[\mathrm{X}]}{\mathrm{d}t} = -k_{\mathrm{d}}([\mathrm{X}] - [\mathrm{X}]_{\mathrm{b}}) \tag{3}$$

Where [X] denotes the species' concentration, and [X]_b represents the background concentration, both expressed in ppb. The parameter k_d was iteratively determined, initially set at 2.2×10^{-5} s⁻¹ Equation 4 was then employed to adjust k_d for subsequent runs. Following several iterations, a stable k_d time series was obtained to best reproduce the CO observation, also measured in ppb, and applied to all species.

$$k_{d \text{ next run}} = k_{d \text{ last run}} * \frac{CO_{last \text{ run}}}{CO_{observation}}$$
(4)

Background concentrations of specific VOC species were obtained from de Gouw et al. (2017, 2018) (refer to Table S2 in Supporting Information S1). Background concentrations of other VOC species and NO_X were set to zero. Free tropospheric O_3 concentrations from 2 to 8 June during the case were acquired from Langford et al. (2012), calculated using the FLEXPART model and verified by O_3 sondes and airborne lidar (Langford et al., 2012). The background concentration for O_3 was essentially bimodal, with fluctuating values during different mornings to represent morning intrusion of residual layer O_3 , and a second constant value was utilized for the remaining time for each day (refer to Figure S3 in Supporting Information S1 for time series of background O_3).

2.5. Emission Rates for Inter-Annual Trend and Sensitivity Test in 2020

To model the inter-annual O_3 trend in LA from 2010 to 2020, emission rates were adjusted annually based on the projected summer anthropogenic emission in LA (Figure S4 in Supporting Information S1), as reported by the California Air Resources Board (CARB) in the California Emissions Projection Analysis Model (CEPAM) 2016 SIP—Standard Emission Tool (California Air Resources Board, 2016). In essence, the emission rates during CalNex 2010 served as the base line, with subsequent years' emissions scaled accordingly. For VOCs, only non-VCP emissions were modified to align with the CO emission trend (California Air Resources Board, 2016). We assume that VCP emissions remained constant due to the absence of targeted regulations for these sources from 2010 to 2020 (Figure 2b). This assumption represents a lower limit on their importance. Weekend NO_X emissions were determined by the average NO_X concentrations ratio observed on weekdays (WD) and weekends (WE) since 2010 (Figure S5 in Supporting Information S1).

The impact of precursor reduction percentages on the percentage change in DMA8 O_3 in 2020 was simulated based on the calculated emissions for 2020, using a 10% gradient for changes in NO_X or non-VCP VOC emissions from 0% to 120%. This test aimed at shaping future pollution mitigation strategies in 2020s.

3. Results and Discussion

3.1. Effects of VCP Emissions on O₃ Episode in 2010

3.1.1. Model Performance and Overall Results

Figure 3 presents the overall results of parallel simulations for two scenarios (with and without VCP emissions) for the CalNex-2010 base case. All settings remain identical between the two scenarios, except the emission ratios of VOCs are either reduced (if that VOC has also sourced other than VCPs) or set to zero (if that VOC is only

CHEN ET AL. 6 of 19

21698996, 2024, 11, Downloaded from https://agupubs.onlinelibrary.wiley.com/doi/10.1029/2024JD040743 by University Of Colorado Libraries, Wiley Online Library on [03/06/2024]. See the Terms

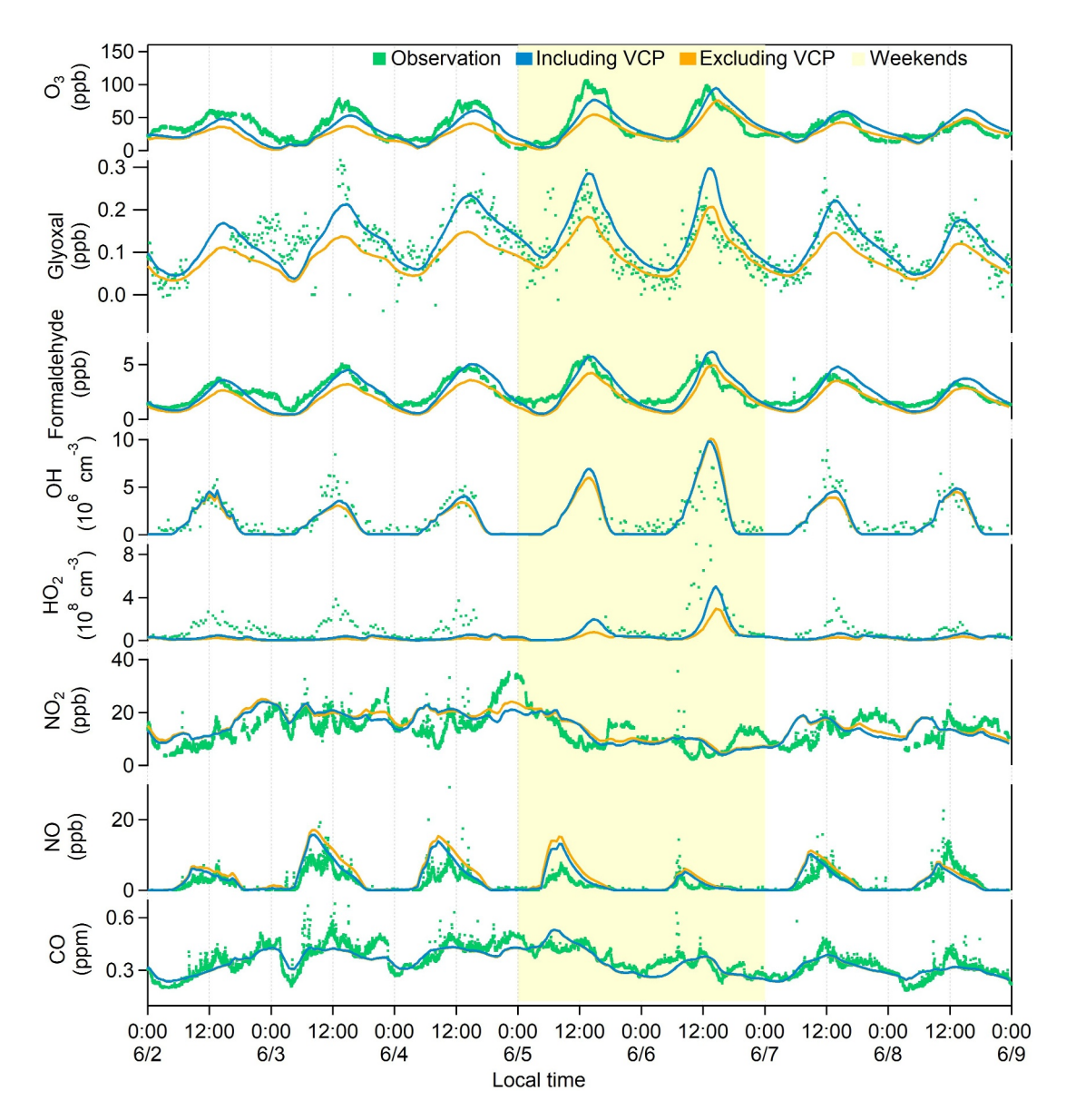


Figure 3. Time series of ozone (O_3) , glyoxal, formaldehyde, OH, HO_2 (70% of HO_2 *), NO_2 , NO_2 , NO_3 , and CO for scenarios with VCP emissions (blue line), scenarios without VCP emissions (orange line), and observations (green points) in the base case. Weekends are indicated by the light-yellow background in the time series.

released from VCPs). After adjusting the first-order physical loss rate for CO, we obtained a reasonable agreement ($r^2 = 0.70$, IOA = 0.90) between simulated CO (0.34 \pm 0.07 ppm) and observed CO (0.36 \pm 0.08 ppm), reflecting the optimized representation of physical dilution.

Upon incorporating VCP emissions, the modeled secondary photochemical products demonstrate good agreement with the observations. When examining O_3 , the IOA increased from 0.77 to 0.88, nearly reaching the upper limit of the previous model studies (0.68–0.89) (Lyu et al., 2016; N. Wang et al., 2015; Y. Wang et al., 2017, 2018). The average O_3 and daily maximum hourly O_3 values were 27 ± 15 ppb and 48 ± 13 ppb without VCP sources, respectively. These values rose to 34 ± 19 ppb and 65 ± 15 ppb in the presence of VCP sources, consistent with the observations (40 ± 20 ppb and 70 ± 20 ppb). VCPs contributed 23% of the DMA8 O_3 (14 ± 3 ppb) during this episode, higher than the average value for the entire summer (17%, 9 ± 2 ppb) as simulated by Qin et al. (2021). The difference may point at an increasing influence of VCPs during O_3 episodes. Hansen et al. (2021) also found that the site was mainly impacted by local anthropogenic emissions from 1 to 8 June compared to the entire observation period. Although glyoxal is not directly released from VCP use, the

CHEN ET AL. 7 of 19

simulated glyoxal result exhibited better agreement with observations after including VCP emissions (simulation: 130 ± 60 ppt, observation: 120 ± 60 ppt, IOA = 0.88). This outcome suggests that the MCM accurately represents the photochemical reactions of VCP species to form glyoxal. The modeled formaldehyde (2.4 \pm 1.5 ppb on average) showed a 32% increase on average due to VCP contributions and was also in good agreement (IOA = 0.90) with the observations (2.5 \pm 1.1 ppb). The weekend effect on O_3 formation (5–6 June) was also captured in the model incorporating VCPs (Figure 3). The IOA value of the simulated weekend O_3 concentration rose from 0.82 to 0.91 after including VCP emissions. While the agreement between modeled and measured O_3 is strongly dependent on several assumptions (dilution rate, free tropospheric O_3 , etc.), the more robust finding of this work is the strong contribution from VCP emissions to O_3 formation.

There were also some notable differences between the model and measurements, for example, for HO₂. The ambient HO₂ concentrations were estimated to be approximately 70% of the measured HO₂* concentrations on average due to RO₂ interference (Griffith et al., 2016). The average simulated HO₂ concentration in this study was $5 \pm 8 \, (\times 10^7 \, \text{molec. cm}^{-3})$, representing 45% of the average measured HO₂ concentrations presented by Griffith et al. (2016). Comparisons were only conducted for periods when observational data were available. Considering the 36% (2 sigma) calibration uncertainty in these measurements (Dusanter et al., 2008), the simulated value is still 19% lower than the actual measurement. The reduction of BVOC concentrations in the model is one of the major reasons. A sensitivity analysis employing observed BVOC concentrations yielded an HO2 mean value of $1.1 \pm 1.8 \,(\times 10^8 \,\mathrm{molec.\,cm}^{-3})$, closely approximating 98% of the average measured value. This result emphasized the significance of nearby-emitted biogenic VOCs in the model's radical budgets. However, as the emissions are local, there has not been sufficient processing time in the atmosphere to build up secondary products like formaldehyde, methyl vinyl ketone and methacrolein, as evidenced in this test (Figure S6 in Supporting Information S1). This suggests that the biogenic VOC emissions at the site aren't fully representative of the wider basin's emissions, unlike the anthropogenic pollutants. Consequently, reducing BVOC concentrations in the model is considered appropriate, especially given its negligible effect on evaluating VCPs' contribution to O₃ formation, which is further explored in the model's uncertainty section.

Another reason is that the model overestimated the NO concentration. The model's underestimation of HO_2 concentration is a common occurrence when NO values exceed a few parts per billion (Brune et al., 2016; Chen et al., 2010; Czader et al., 2013; Dusanter et al., 2009; Emmerson et al., 2005, 2007; Griffith et al., 2016; Kanaya et al., 2007; Ren et al., 2013; Sheehy et al., 2010; Shirley et al., 2006). We utilized a scenario with a 20% reduction in NO_X emission to evaluate this issue (Figure S7 in Supporting Information S1). The result demonstrated that the simulated NO level was comparable to measurement, and the modeled average HO_2 reached 64% of the measured HO_2 . However, the 20% reduction in NO_X emissions only resulted in a 6% and 5% overestimation of observed DMA8 O_3 , respectively. This shows that the simulated HO_2 concentration can almost sustain the formation of the observed O_3 concentration. Shirley et al. (2006) suggested that some products of the reaction between HO_2 and NO were not OH and NO_2 . Furthermore, the sensitivity test also shows that a 20% reduction in NO_X emission did not strongly affect the contribution of VCP to O_3 formation rates (from 1.1 \pm 1.3 ppb $^{-1}$ to 1.2 \pm 1.4 ppb hr^{-1} during 7:00-17:00) and L_{OH} (both 2.4 \pm 0.8 s $^{-1}$). Therefore, the difference between the simulated and measured HO_2 has a limited impact on the overall conclusions of this study.

Multiple factors can contribute to the uncertainty of the overall model results. The first one concerns the accurate characterization of key VCP species' chemical processes in the MCM, which involves two aspects: the mapping relationship between VOC species and MCM surrogates and the representativeness of MCM surrogates' reaction processes. The impact of VOC species on OH reactivity was determined by multiplying the k_{OH} by the species' emission ratio. The ER* k_{OH} value for MCM surrogates was only 4% higher than that of all VOCs in the VCP emission inventory, suggesting that the mapping relationship had a negligible effect on the overall R_{OH} . Figure 4 displays the ranking of ER* k_{OH} values for groups/species in the VCP emission inventory. Key species include limonene, isopropanol, ethanol, propylene glycol, and ethylene glycol, which collectively contributed 63% of the VCP ER* k_{OH} value. All these species are explicitly included in the MCM, suggesting that the reaction processes of major VCP species are adequately represented in MCM.

The second factor is the uncertainty of NO_X emissions. As previously mentioned, a 20% reduction in NO_X emissions would improve the simulations of O_3 and NO (Figure S7 in Supporting Information S1). However, this would not affect the contribution of VCP to O_3 formation rate and R_{OH} , and no further evidence supports this adjustment. The third factor pertains to the influence of BVOC. As discussed in Section 2.4 and in overall results,

CHEN ET AL. 8 of 19

OH reactivity Fraction

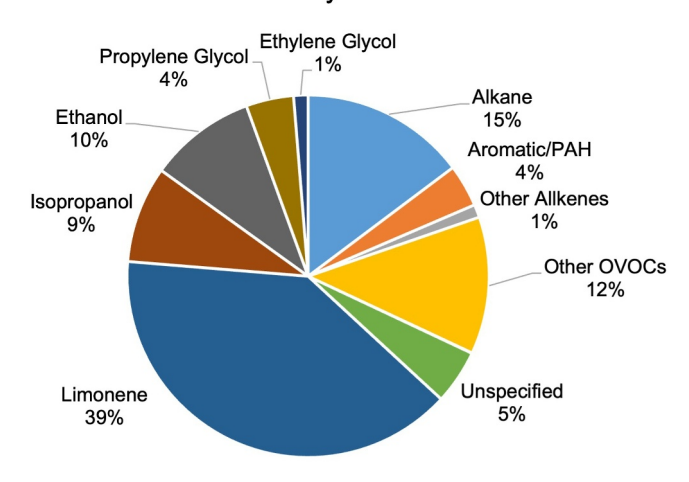


Figure 4. Breakdown of the OH reactivity in VCP. "Unspecified" includes oxy IVOCs and non-oxy IVOCs. "Limonene" includes D-limonene, Dl-limonene, Fragrances, and Pine oil (McDonald et al., 2018).

the sampling location might have been affected by emissions from nearby biogenic sources. The simulated results of BVOC concentrations sensitivity demonstrate that the contribution of VCP to DMA8 O_3 was 13 ± 5 ppb, only marginally different from the simulation results of one-sixth BVOC (14 \pm 3 ppb). This result indicates that the uncertainty of BVOC has a negligible impact on our findings regarding the contribution of VCP emissions to O_3 . This issue will be discussed further in the discussion of R_{OH} in the next section. In general, the MCM chemical mechanism can effectively characterize the significant impact of VCP emissions on O_3 chemistry.

3.1.2. OH Reactivity

This study also analyzed the R_{OH} to evaluate the representation of VCPs in the model. In the base case, the R_{OH} was $13.1\pm1.8~{\rm s}^{-1}$. In comparison, using the original measured biogenic VOC concentrations (rather than reducing it to one-sixth in base case), the R_{OH} reached $16\pm5~{\rm s}^{-1}$ (Case A in Table 1). This value nearly matched the observations (21 s⁻¹) measured by Hansen et al. (2021) considering the measurement uncertainty (25%). Fossil fuel emissions and other non-VCP sources accounted for 62% of the measured R_{OH} , which is higher than the CalNex-2010 results simulated by McDonald et al. (2018) (53%). The primary difference stemmed from the contribution of

nearby biogenic emissions (10%). Although locally emitted biogenic VOCs affected the observed radical concentrations and loss rates, their impact on the formation of O_3 and other secondary products (e.g., formaldehyde, methyl vinyl ketone, methacrolein) may have been minimal as these are formed on much longer timescales.

Disturbances from biogenic sources near the sampling location mainly influenced the R_{OH} contributed by non-VCP fractions (from $11\pm3~{\rm s}^{-1}$ to $13\pm4~{\rm s}^{-1}$), with negligible effects on the R_{OH} contributed by the VCP (from $2.4\pm0.8~{\rm s}^{-1}$ to $2.5\pm0.8~{\rm s}^{-1}$). McDonald et al. (2018) indicated that by incorporating a 23% contribution from VCP, the modeled OH reactivity (16.0 ${\rm s}^{-1}$) is in good agreement with the observations from CalNex-2010 (21 \pm 7 ${\rm s}^{-1}$), considering the uncertainty involved. In our study, VCP use contributed $2.5\pm0.8~{\rm s}^{-1}$ to the R_{OH} , constituting only 12% of the total measured R_{OH} . This result is comparable to the R_{OH} modeled by Qin et al. (2021) in a CTM for the same observation experiment (2.7 ${\rm s}^{-1}$, 13% of the measured R_{OH}) based on individual VOC species.

The difference with the R_{OH} values calculated by McDonald et al. (2018) for the VCP contribution can be explained by several factors. The first factor is dry deposition, which is highly uncertain for OVOCs. Karl et al. (2018) found minor influences of dry deposition on VOCs in urban areas; however, these findings were based on areas with limited vegetation, such as central Innsbruck (Peron et al., 2024). In contrast, Los Angeles, characterized by its sprawling suburban landscape and abundant tree cover, likely experiences higher rates of dry deposition for OVOCs, as indicated by recent studies like those of Pfannerstill et al. (2023). To incorporate this variability, we applied strong dry deposition velocities of VOCs (predominantly OVOCs) from Zhang et al. (2003) in our model. This approach led us to conduct a sensitivity test by omitting dry deposition of VOCs. The test revealed that excluding deposition resulted in a notable increase in R_{OH} values for both VCPs and other

Table 1
OH Reactivity From McDonald et al. (2018), Qin et al. (2021), and in This Work

| Туре | Basic case | A | В | McDonald et al., 2018 | Qin et al., 2021 ^a |
|-----------------------------------|------------------|------------------|------------------|-----------------------|-------------------------------|
| Duration | 2 to 8 June 2010 | 2 to 8 June 2010 | 2 to 8 June 2010 | CalNex-2010 | CalNex-2010 |
| Observation | 21 ± 7 | 21 ± 7 | 21 ± 7 | 21 ± 7 | 21 |
| Total R _{OH} by modeling | 13 ± 4 | 16 ± 5 | 14 ± 4 | 16.0 | 14.3 |
| Use of VCPs | 2.4 ± 0.8 | 2.5 ± 0.8 | 2.7 ± 0.9 | 4.8 ± 3.4 | 2.7 |

Note. Base case: Includes VCP emissions and BVOCs lower than measured values. Case A: BVOC concentrations adjusted to 100% of measured values. Case B: Dry deposition of VOCs removed. ^aThe results from Qin et al. (2021) here are the results of calculations based on subdivided VOC species in the text.

CHEN ET AL. 9 of 19

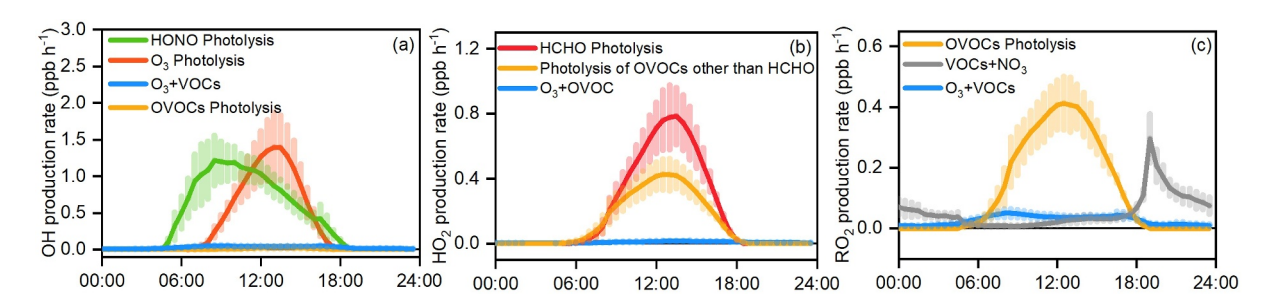


Figure 5. Average diurnal variations of primary production rates of (a) OH, (b) HO₂, and (c) RO₂ in the simulation results of the base case with VCP emissions added. The error bars indicate the standard deviations of the mean.

VOC sources (13% and 7% higher than the base setting, respectively), as shown in Case B of Table 1. This finding underlines the significant role of dry deposition in VOC dynamics. Particularly noteworthy is ethanol, which emerges as the most substantial VOC emitter in both scenarios and a key component of VCPs. We examined its dry deposition impact, revealing substantial effects on both concentration (average 6.5 \pm 1.6 ppb without deposition vs. 3.1 \pm 1.9 ppb with deposition, Figure S8 in Supporting Information S1) and R_{OH} (0.8 \pm 0.2 s⁻¹ vs. 0.5 \pm 0.1 s⁻¹). The test underscores the importance of considering dry deposition in the model when evaluating VCP's impact on R_{OH} .

The second factor is the mapping of chemical species into MCM, which was already discussed above. The third one is the reactions of olefins and terpenes with O_3 . The box model of McDonald et al. (2018) did not consider these reactions. We attempted to turn off the reactions of olefins and terpenes with O_3 in our model. Since O_3 is an important oxidant for olefins at night (de Gouw et al., 2017), turning off these reactions would substantially increase R_{OH} at night. Taking this into account, we primarily compared the results of the tests during the daytime (5:00 to 17:30). The results demonstrate that ignoring these reactions can increase the R_{OH} of VCP by 1.0 s^{-1} during the daytime compared to the daytime average of base case ($2.5 \pm 0.5 \text{ s}^{-1}$), reaching $3.5 \pm 1.1 \text{ s}^{-1}$ and contributing 15% of the daytime R_{OH} in this case. Therefore, it is considered that the reactions of olefins and terpenes with O_3 are one of the main reasons for the large differences in quantification results. Additionally, the application of different modeling methods could also cause discrepancies. McDonald et al. (2018) use a box model considering the consumption of VOC by measured OH, while our model uses a near explicit mechanism without constraining OH. Despite those differences, both studies report results that are consistently lower than the respective average values measured during their study periods. This consistent underestimation would imply an underestimation of O_3 chemistry influenced by VCP and suggest a further update of the model.

3.1.3. Radical Chemistry

The effect of VCP on O_3 chemistry was investigated in more detail through the modeled radical budgets. The model demonstrated strong correspondence with measured OH radical concentrations in both scenarios (mean and IOA: 2 ± 2 (×10⁶ molec. cm⁻³) and 0.91 with VCP, 2 ± 2 (×10⁶ molec. cm⁻³), and 0.90 without VCP). As discussed above, including VCP emissions enhanced the simulated values for HO₂, raising the average concentration from 3 ± 5 (×10⁷ molec. cm⁻³) to 5 ± 8 (×10⁷ molec. cm⁻³), and the IOA value increased from 0.53 to 0.67. Nonetheless, this enhancement was limited, and the simulated values for HO₂ are still much lower than the observed HO₂ concentration (1.1 \pm 1.3 (×10⁸ molec. cm⁻³)), indicating insufficient representation of peroxyl radicals. Potential explanations involve biogenic emission, unmeasured secondary products of high oxidation states, overestimated NO_x concentrations, and unidentified chemical reaction processes (Section 3.1.1).

Figure 5 displays the average daily variations of the primary production rate of RO_X (OH, HO_2 and RO_2) in the scenario incorporating VCP emissions. OVOC photolysis constituted the largest primary source of RO_X radicals during the daytime, contributing 0.6 ± 0.5 ppb hr^{-1} of HO_2 radicals (0.4 ± 0.3 ppb hr^{-1} from formaldehyde photolysis) and 0.2 ± 0.2 ppb hr^{-1} of RO_2 . HONO photolysis and O_3 photolysis ranked the second and third largest among primary sources of daytime RO_X radicals, contributing 0.8 ± 0.4 ppb hr^{-1} and 0.6 ± 0.6 ppb hr^{-1} to OH radicals, respectively. Figure 6 illustrates the contributions of VCP to the primary sources of RO_X radicals, which were calculated as the differences between the two scenarios with and without VCP emissions. The extent of the VCP contribution to the primary sources of RO_X was temporally proportional to the total rate of primary

CHEN ET AL. 10 of 19

21698996, 2024, 11, Downloaded from https://agupubs.onlinelibrary.wiley.com/doi/10.1029/2024JD040743 by Univ

and-conditions) on Wiley Online Library for rules of use; OA articles are governed by the applicable Creati

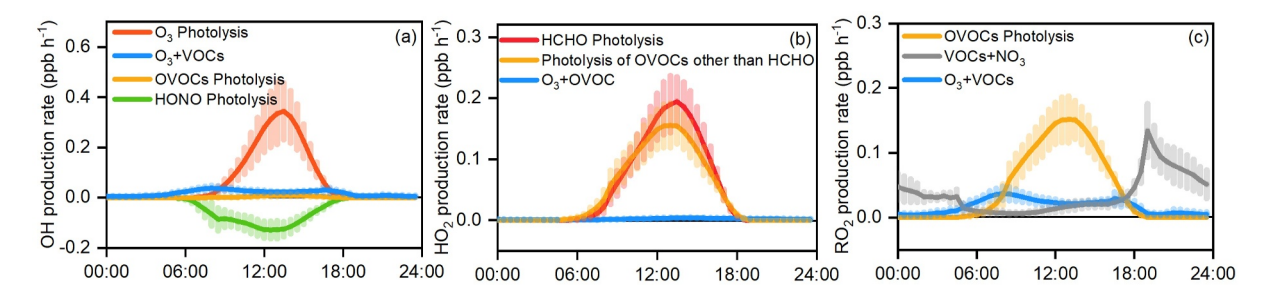


Figure 6. The difference of primary radical sources between scenarios including and excluding VCPs for (a) OH, (b) HO₂, and (c) RO₂. The solid lines indicate the diurnal variations. The error bars indicate the standard deviations of the mean.

sources of RO_X radicals. The VCP contribution to the daytime average primary production rates of OH, HO_2 , and RO_2 radicals was 0.09 ± 0.10 ppb hr^{-1} (6%), 0.17 ± 0.13 ppb hr^{-1} (28%), and 0.12 ± 0.06 ppb hr^{-1} (41%), respectively, suggesting that VCP makes an important contribution to the primary source of HO_2 and RO_2 radicals. Given the limited contribution of VCP to primary OH production rates, this result also explains the similar OH radical concentrations between the two scenarios. Additionally, introducing VCP speeds up NO_X 's loss through alkyl nitrates, diminishing NO_X levels. This results in reduced HONO formation via NO_2 -related reactions, leading to a subtle decline in HONO-to-OH photolysis.

Figures 7 and 8 reveal the photochemical impacts of VCP from the perspective of RO_X radical recycling. As shown in Figure 7, radical recycling was efficient in the base case, with a rate about five times faster than the primary production rate. Regarding radical termination reactions, the reaction of RO_X radicals with NO_X (i.e., OH + NO_2 and RO_2 + NO_2) prevailed, attributed to the elevated NO_X concentrations in polluted urban areas (Tan et al., 2019). Figure 8 presents the production, recycling, and removal rates of RO_X contributed by VCP, which

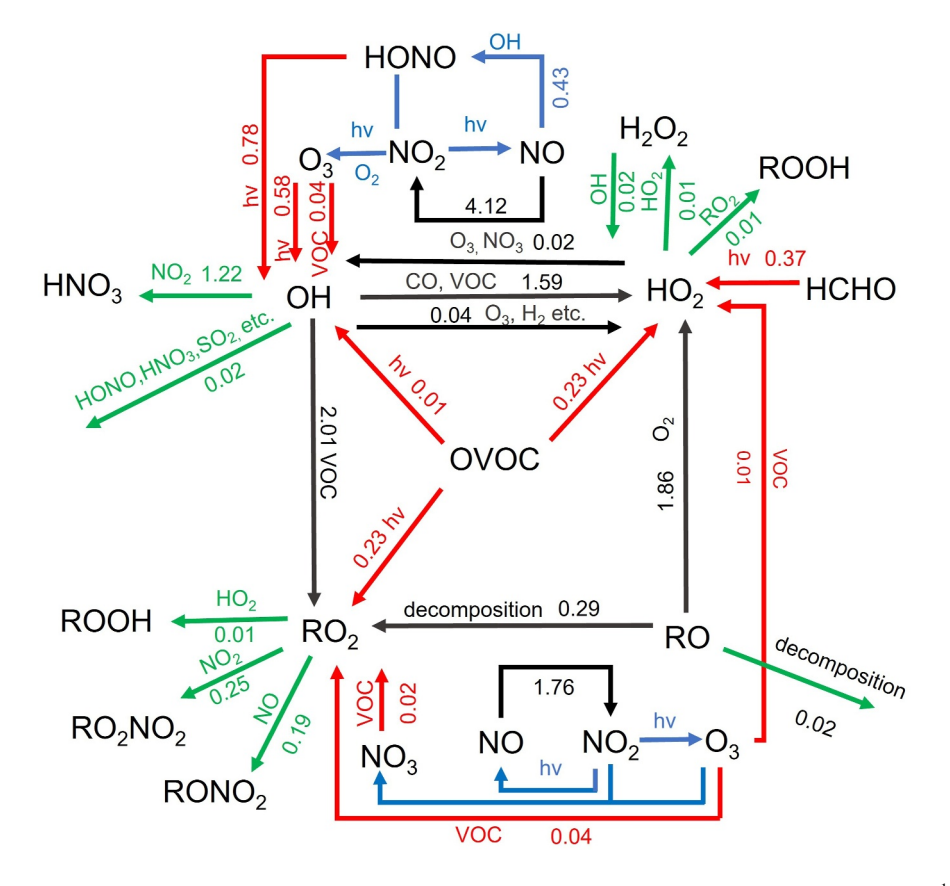


Figure 7. Results of daytime average RO_X budget simulation for the base case with VCP emissions added (in ppb h⁻¹). The red, black, and green lines indicate the primary production, recycling, and termination pathways of radicals, respectively.

CHEN ET AL.

2024, 11, Downloaded from https://agupubs.onlinelibrary.wiley

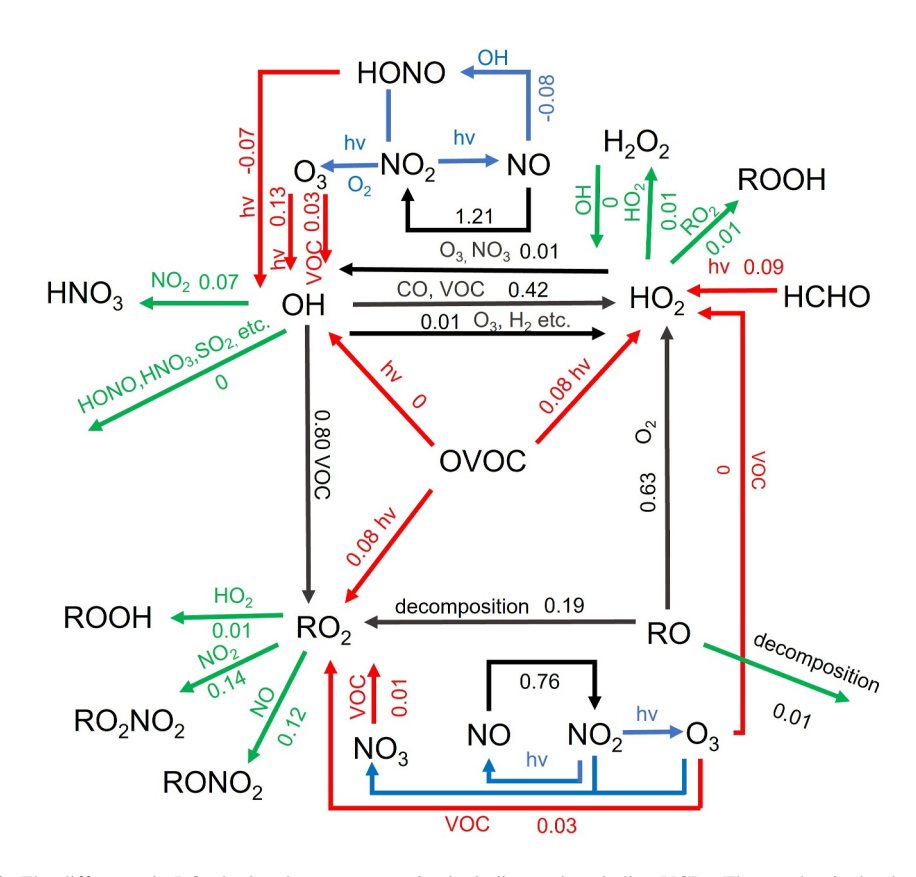


Figure 8. The difference in RO_X budget between scenarios including and excluding VCPs. The number is the daytime average rates (in ppb h^{-1}). The red, black, and green lines indicate the primary production, recycling, and termination pathways of radicals, respectively.

were defined as the differences between the two scenarios with and without VCP. The radical recycling rate contributed by VCP was nearly 11 times faster than the primary production rate, signifying a more efficient acceleration of radical recycling by VCP species. The radical recycling rate contributed by VCP was also 11 times faster than the radical removal rate, surpassing the corresponding ratio in the base case (7 times), indicating that VCP-produced radicals need to undergo more reactions and produce more O_3 before they exit the RO_X radical cycle. The change in the NO_2 formation rate (oxidation of NO by HO_2 and RO_2 radicals) corroborated this conclusion. Incorporating VCP raised the rate of $NO \rightarrow NO_2$ by 2.0 ± 1.3 ppb hr⁻¹, which equates to 33% more O_3 being produced from daytime radical recycling. The heightened efficiency of radical recycling can be explained by the composition of the VCP species, which primarily comprise OVOCs and unsaturated VOCs with higher reactivity. Moreover, the analogous OH concentrations between the two scenarios can also be explained by RO_X radical recycling. Adding VCP emissions resulted in a more efficient radical recycling process, with daytime reaction rates of $HO_2 \rightarrow OH$ and $OH \rightarrow RO_2$ increased by 30% and 40%, respectively. In contrast, the net rate of OH production through mutual reactions increased by only 6%, leading to accelerated formation of oxidation products with a minor change in OH concentration.

3.1.4. O₃ Formation Mechanism

The diurnal variation of O_3 formation and loss rates is depicted in Figure 9a. As indicated by the black solid and dashed lines, the net daytime O_3 production rate $(5.6 \pm 4.1 \text{ ppb hr}^{-1})$ was visibly accelerated by VCP, with 39% of the rate originating from VCP's contribution $(2.2 \pm 1.5 \text{ ppb hr}^{-1})$. Figure 9b displays the contribution of VCP to each pathway of the O_3 chemical budget (the contribution to the loss pathway is indicated as a negative value). VCP contributed 29% and 39% to the total rates of NO reactions with HO_2 and RO_2 , indicating its significant chemical impact.

CHEN ET AL. 12 of 19

21698996, 2024, 11, Downloaded from https://agupubs.onlinelibrary.wiley.com/doi/10.1029/2024JD040743 by University Of Colorado

onditions) on Wiley Online Library for rules of use; OA articles are governed by the applicable Creati

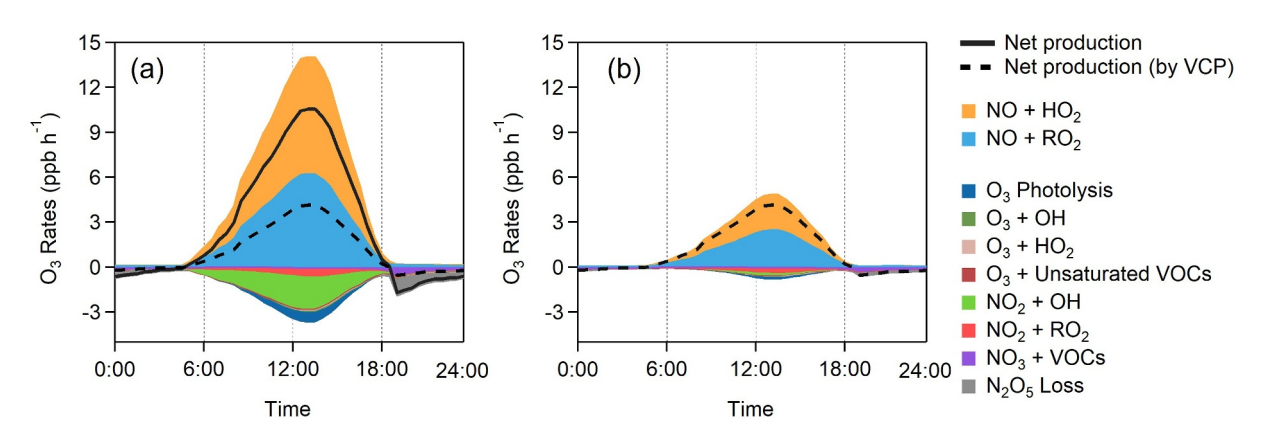


Figure 9. (a) Breakdown of chemical production and loss rates of O₃ during 2–8 June 2010; (b) the same to (a) but for the contributions from the VCPs.

3.2. O₃ Formation in Lumped Mechanisms: Implication for Regional Modeling of VCP Emissions

Next, we study how well VCP oxidation and its effect on O_3 formation are represented in lumped mechanisms. Figure 10 displays the results obtained with other, more computationally efficient chemical mechanisms used in CTMs. This comparison excludes dry deposition except for O_3 , NO_2 , HNO_3 , HONO, and PAN. As shown in Figure 10, average DMA8 O_3 concentrations for MCMv331 (62 \pm 13 ppb), RACM2 (58 \pm 13 ppb) and SAPRC07B (59 \pm 14 ppb) are comparable with the differences within 6% and 5%, respectively. The simulation results of RACM2-VCP (65 \pm 13 ppb) were 4% higher than those of MCM (3 \pm 1 ppb). In contrast, CB6r2 (37 \pm 10 ppb) exhibited 59% of O_3 concentration of MCM. The differences in formaldehyde simulated by various mechanisms were insignificant, except for CB6r2 (50% lower than MCM). The discrepancies in OH concentration simulated by RACM2-VCP, SAPRC, and MCM was minor (between -7% and 2% compared to MCM), but the difference with CB6r2 was substantial (45%), too.

These mechanisms also varied in their representation of VCP R_{OH} (Figure S9 in Supporting Information S1). CB6r2 demonstrated the lowest R_{OH} for VCP (1.0 \pm 0.4 s⁻¹). The VCP R_{OH} for RACM2 and SAPRC07B were

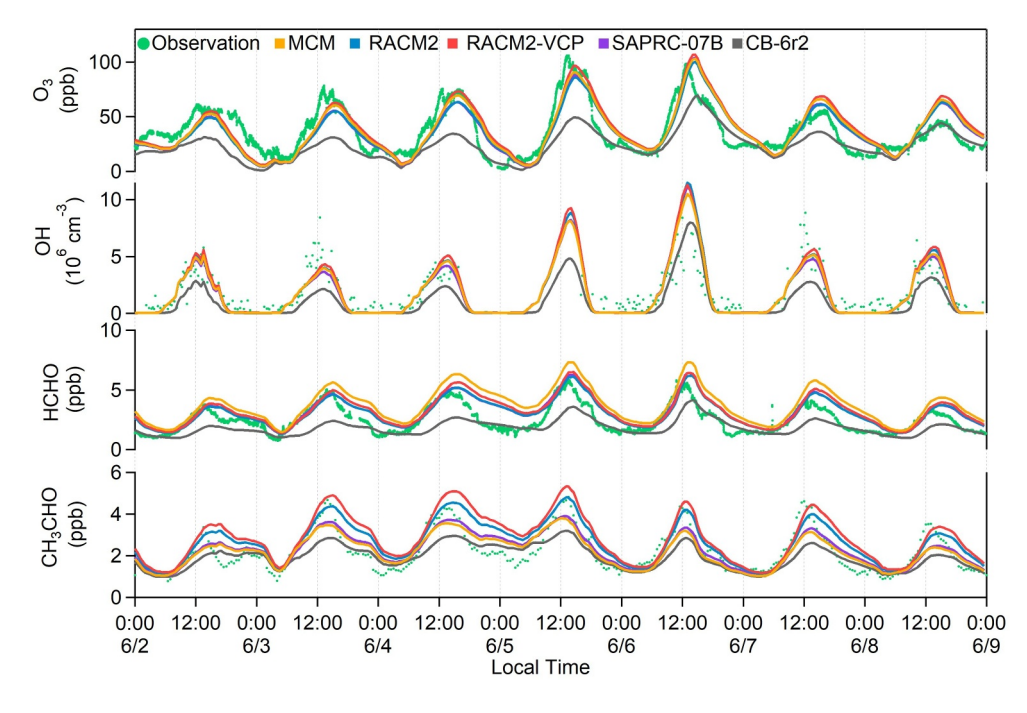


Figure 10. Concentrations of O_3 , OH radical, formaldehyde and acetaldehyde from observation and simulated by MCM, RACM2, RACM2-VCP, SAPRC-07B and CB-6r2 with VCP emissions. Those simulation exclude dry deposition except for O_3 , NO_2 , HNO_3 , HONO, and PAN.

CHEN ET AL. 13 of 19

identical $(1.8 \pm 0.7~{\rm s}^{-1})$, which were lower than MCM $(2.7 \pm 0.9~{\rm s}^{-1})$. In comparison, the $R_{\rm OH}$ in RACM2-VCP $(2.3 \pm 0.9~{\rm s}^{-1})$, which incorporates and updates the reaction mechanism of the key VCP species, deviated less from that of MCM (15%). Expectedly, the relative differences in presenting VCP $R_{\rm OH}$ for several chemical mechanisms were consistent with those in their simulated O_3 concentrations. These variations can be partially explained by the difference between the $ER*k_{\rm OH}$ values of the surrogates in these lumped mechanisms and in the MCM. When looking at the VCP emissions, the deviation of the $ER*k_{\rm OH}$ values of RACM2-VCP from the reference values was -2% compared to -11% for RACM2, indicating that RACM2-VCP effectively enhanced the capability of the model for VCP chemistry. The deviation of the $ER*k_{\rm OH}$ of VCP emissions for SAPRC07B reached -36%. Concerning total $ER*k_{\rm OH}$, the deviation of RACM2-VCP was 1%, which was superior to RACM2 (-4%) and SAPRC (-17%) and equivalent to MCM.

The analysis suggests that the RACM2-VCP mechanism is a suitable choice for simulating VCP chemistry in CTM concerning O₃ formation. RACM2 and SAPRC are less appropriate, and CB6r2 is least reliable. The weak performance of CB6r2 can be attributed to the less detailed isoprene chemistry (Dunker et al., 2016) and the use of non-integer product coefficients (Luecken et al., 2019). Overall, the incorporation of key species such as propylene glycol, isopropanol, glycerol, as well as updates for ethanol, methanol, acetone, and ethylene glycol, as detailed in the RACM2-VCP, significantly improves our simulations, making them more akin to the near-explicit chemical mechanism in terms of accuracy and detail. Nonetheless, it is important to note that key reactive species may vary across regions due to differences in emissions. Consequently, evaluating local VCP emission inventories for various regions remains crucial for obtaining more accurate simulation and provide targeted suggestions for O₃ control. In addition, this model can be used to test the effects of other mechanisms in representing VCP chemistry.

3.3. Inter-Annual Trend

As stated in the Introduction, O_3 concentrations in Pasadena have exhibited a slightly upward trend since around 2010. Based on the good representation of an O_3 episode in 2010, we further use the model to study the impact from VCPs by examining O_3 trends in Pasadena since 2010. As previously described, VOC emissions from VCP are assumed to have remained constant over this decade. NO_X and non-VCP VOC emissions are presumed to have decreased in accordance with CARB emission inventories. NO_X emissions on weekends were scaled based on the ratio of average NO_X concentrations observed on weekdays and weekends since 2010. We continued to use the MCM mechanism here, as RACM2-VCP's results overestimated the trend, possibly due to its oversimplified OVOC deposition scheme.

Figures 11a-11c depict the observed and simulated DMA8 O_3 inter-annual trends for all days, weekdays, and weekends normalized to the 2010 average. As shown in Figure 11a, including VCP emissions accounted for the trend in the measurements within the uncertainties. Given that the weekend O_3 effect is a crucial test case for O_3 inter-annual trend modeling, the data were further divided into weekdays (Figure 11b) and weekends (Figure 11c). On weekdays, the model and observations were in good agreement, staying within the margin of uncertainties. Over the weekends, the model successfully captured the slight decrease in the trend, though some data points fell outside the expected uncertainty range. The discrepancies on weekends may stem from a missing weekend inter-annual trend of VOC emissions. In combination, these results lend further credence to the representation of O_3 chemistry in the model and suggest that VCP has played a significant role in the O_3 trends in Pasadena since 2010. Additional research on VCP emissions on weekends and weekdays may help elucidate the decreasing trend in weekend O_3 since 2010.

Figures 11d–11f present the normalized inter-annual DMA8 O_3 trends under simulated conditions of less-than-actual emission reductions, with emissions set at 120% of actual levels. This analysis focuses on three separate contributors: NO_X , non-VCPs, and VCPs. Figure 11d reveals that actual NO_X emission reductions, compared to a hypothetical larger emission scenario (120% NO_X), resulted in a higher average trend (1.05 vs. 0.98). However, it simultaneously led to a reduced trend slope (0.0016/year vs. 0.0178/year). In contrast, the actual condition in non-VCP emissions significantly lowered the average trend level (1.05 vs. 1.16) and increased its slope (0.016/year vs. 0.0099/year). When these findings are considered alongside the emission trends depicted in Figure S4 in Supporting Information S1, it becomes clear that the slight increase in the O_3 trend slope during the 2010s is primarily due to the rapid reduction in NO_X emissions, accompanied by a more gradual decline in VOC emissions. Moreover, actual VCP emissions, in comparison to the hypothetical higher emission scenarios, led to a similar

CHEN ET AL. 14 of 19

21698996, 2024, 11, Downloaded from https://agupubs.onlinelibrary.wiley.com/doi/10.1029/2024JD040743 by University Of Colorado Libraries, Wiley Online Library on [03/06/2024]. See the Terms and Condition

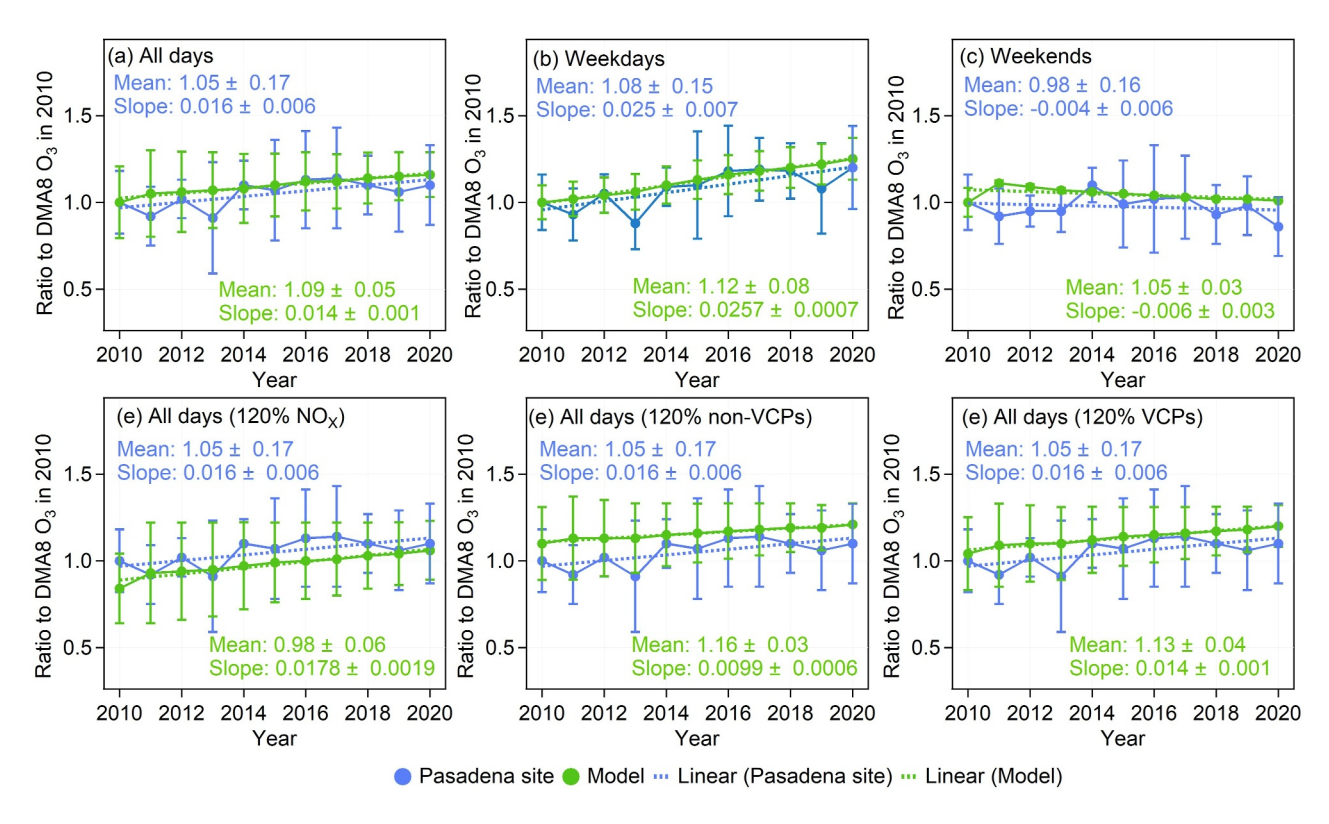


Figure 11. Inter-annual trends in DMA8 O_3 ratios relative to 2010 for (a) all days, (b) weekdays, and (c) weekends in June (error bars represent one standard deviation). In the model, VOC emissions from VCP are assumed to remain constant throughout the decade. Both NO_X and non-VCP VOC emissions are believed to have decreased in line with CARB emission inventories. NO_X emissions on weekends were adjusted based on the ratio of average NO_X concentrations observed between weekdays and weekends post-2010. The recorded O_3 concentration was measured at the Pasadena site. (d), (e), and (f) depict the impacts on O_3 trends of a 20% increase in emissions for NO_X , non-VCP VOCs, and VCP VOCs, respectively. The results in panels (d), (e), and (f) were all normalized to the all-days' results in 2010 in the base model.

decrease in the mean trend level (1.05 vs. 1.13) but with a slightly less pronounced increase in the trend's slope (0.016/year vs. 0.014/year) when compared with non-VCPs. This indicates that reducing VCP emissions will not only decrease the mean value of the trend but also lead to a slightly smaller increase in the slope compared to non-VCPs.

3.4. Potential Emission Control Strategy for 2020s

Leveraging the model's good depiction of Pasadena's O_3 trend from 2010 to 2020, we analyzed the effects of emission reductions for 2020. This year's settings, as shown in the interannual trend analysis, were chosen as the baseline, illustrated by the red point in Figure 12. NO_X and non-VCP VOC emissions were independently altered in 10% increments, ranging from 0% to 120%, while keeping the other constant, as indicated by the orange points (for NO_X) and blue points (for non-VCP VOCs) in Figure 12. Each point's simulated DMA8 O_3 level was normalized to this baseline. Figure 12 reveals these results, highlighting the typical summer urban O_3 pattern in 2020, marked by sensitivity to VOCs and an approach toward NO_X saturation. The findings suggest that O_3 production was nearing its peak with NO_X , while VOC reductions were notably influencing O_3 levels. Nonetheless, the COVID-19 pandemic's impact on emissions in 2020 and beyond, not fully reflected in the emission inventories, introduces uncertainties in the analysis of this data. Furthermore, the 22% contribution of VCPs to the baseline DMA8 O_3 in 2020 significantly exceeded the findings for LA in the summer of 2021 reported by Zhu et al. (2023). Such a discrepancy points to potential differences in emission inventories and meteorological conditions.

Acknowledging the discrepancy and unaccounted factors such as the COVID-19 pandemic in our emission calculations, we extended our analysis by comparing our emission rates with data from the RECAP-CA (Re-Evaluating the Chemistry of Air Pollutants in California) aircraft campaign conducted in June 2021 over Los Angeles and the Central Valley (Nussbaumer et al., 2023). Our base scenario showed median NO_X emission rates

CHEN ET AL. 15 of 19

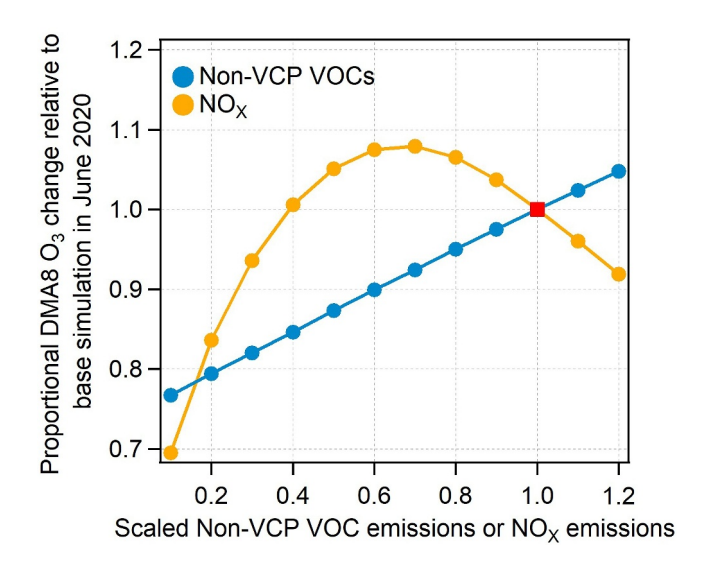


Figure 12. Proportional DMA8 O_3 change relative to base simulation in June 2020 due to the proportional reduction of precursors in 2020 simulated by the model. The red point represents the setup in 2020 derived from the interannual trend, serving as the starting point. NO_X or non-VCP VOC emissions were scaled using a 10% gradient from 0% to 120%, while another group remained constant, illustrated by the orange and blue points, respectively. Each point's DMA8 O_3 have been normalized to the value of base point.

of 0.52 mg N m⁻² hr⁻¹ for weekdays and 0.26 mg N m⁻² hr⁻¹ for weekends. In contrast, RECAP-CA observed median NO_X fluxes in Downtown Los Angeles at 0.27 and 0.12 mg N m⁻² hr⁻¹ for weekdays and weekends, respectively (Nussbaumer et al., 2023). The NO_X emissions calculated from the inventory were generally higher than RECAP-CA's measurements, a finding corroborated by Nussbaumer et al. (2023). This discrepancy likely arises from COVID-19-related changes and overall emission reductions not yet captured in the emission inventory (Nussbaumer et al., 2023). Furthermore, in our 2020 base case, the average emission rate of ethanol (the primary VOC) from 11:00 to 17:00 was 1.12 \pm 0.01 mg m⁻² hr⁻¹. This figure is less than the observed flux during RECAP-CA by a factor of 3.4, which was 3.8 \pm 12.9 mg m⁻² hr⁻¹. This underestimation by CARB was also highlighted by Pfannerstill et al. (2023), suggesting potential missing sources of OVOCs in the inventory.

Adjusting our 2020 NO_X emissions estimates to reflect 2021 observation (50% reduction), as demonstrated in Figure 12, results in a shift in the O_3 formation regime: from NO_X -saturated to NO_X -limited. This recalibration suggests a less prominent role for VCPs in influencing DMA8 O_3 levels in 2020 (9%), consistent with the results from Zhu et al. (2023). These results suggest that from 2010 to 2020, as NO_X emissions were reduced, the range of VCPs' contribution to O_3 concentrations also decreased. Nonetheless, the future trend of NO_X emissions is clouded with uncertainties, influenced by factors like economic recovery, increased trucking due to online retail, and the adoption of electric vehicles, potentially leading to fluctuations in NO_X 's impact on O_3 production. These oscillations could complicate shaping

effective control strategies. Meanwhile, the underestimation of OVOCs could not change the conclusion that an emission reduction strategy targeting VOCs could lead to further O_3 reduction in 2020s. Given the uncertain trends in NO_X emissions and their fluctuating impact on O_3 levels in LA, addressing VCP emissions is crucial for transitioning the O_3 formation regime and buffering the oscillating effect of NO_X .

4. Conclusion

In CalNex-2010 study, using an emission-based box model, we determined that VCP significantly influenced atmospheric photochemistry and O_3 formation. The modeled OH reactivity aligned well with observation when factoring in VCP emissions. VCP emerged as a crucial contributor to the primary RO_x radical source and its recycling. Among various modeling mechanisms evaluated, RACM2-VCP demonstrated the highest alignment with MCM, endorsing it as a preferred choice for regional transport models. Intriguingly, despite reductions in NO_X and VOC emissions in LA since 2010, O_3 concentrations have persistently remained high. Model results generally mirrored the observed patterns, indicated that the slight increase in the O_3 trend slope during the 2010s is primarily due to the rapid reduction in NO_X emissions, accompanied by a more gradual decline in VOC emissions (including contribution from VCPs).

Given the impact of COVID-19, an analysis of 2020 emissions in LA reveals a shift to a NOx-limited O_3 formation regime, thereby diminishing the influence of VCPs on DMA8 O_3 . However, the future trends of NOx remain uncertain. Simultaneously, the importance of VCP emissions is rising. Addressing VCP emissions is crucial for a stable transition in the O_3 formation regime. This approach effectively buffers against the oscillating impact of NOx. While this analysis is specific to Los Angeles, the insights may be relevant to other US cities undergoing similar transitions.

Data Availability Statement

A fuel-based inventory by S.-W. Kim et al. (2016) provided the CO and NO_X emission rates. Observed emission ratios were reported by de Gouw et al. (2017, 2018). The volatile chemical product emission inventory was developed and proposed by McDonald et al. (2018). The California Air Resources Board (CARB) reported on

CHEN ET AL. 16 of 19

LA's inter-annual anthropogenic emissions, detailed in the California Emissions Projection Analysis Model (CEPAM) 2016 SIP-Standard Emission Tool (California Air Resources Board, 2016). Background concentrations of specific VOC species were obtained from de Gouw et al. (2017, 2018). Langford et al. (2012) provided data on free tropospheric O₃ concentrations. The observation data from the CalNex study is available in the NOAA data archive (National Oceanic and Atmospheric Administration, 2010). Data on the inter-annual trends of O₃ and NO₂ observations can be requested from the corresponding author. The Framework for 0-D Atmo-

Acknowledgments

This work was funded by US National Science Foundation (Grant 2206655 to J. G.), the National Science Foundation of China (grants 42061160478 to L.X.).

References

spheric Modeling (F0AM) is available from Wolfe et al. (2016). The observation data, emission ratios, interannual emission trends, and mapping tables have been deposited at (Chen, 2024).

- Brune, W. H., Baier, B. C., Thomas, J., Ren, X., Cohen, R. C., Pusede, S. E., et al. (2016). Ozone production chemistry in the presence of urban plumes. Faraday Discussions, 189(0), 169-189. https://doi.org/10.1039/C5FD00204D
- Cai, C., Kelly, J. T., Avise, J. C., Kaduwela, A. P., & Stockwell, W. R. (2011). Photochemical modeling in California with two chemical mechanisms: Model intercomparison and response to emission reductions. Journal of the Air and Waste Management Association, 61(5), 559-572. https://doi.org/10.3155/1047-3289.61.5.559
- California Air Resources Board. (2016). Cepam: 2016 SIP Standard emissions tool. Retrieved from https://www.arb.ca.gov/app/emsinv/ fcemssumcat/fcemssumcat2016.php
- Carter, W. P. L. (2010). Development of the SAPRC-07 chemical mechanism. Atmospheric Environment, 44(40), 5324-5335. https://doi.org/10. 1016/j.atmosenv.2010.01.026
- Chen, S., Ren, X., Mao, J., Chen, Z., Brune, W. H., Lefer, B., et al. (2010). A comparison of chemical mechanisms based on TRAMP-2006 field data. Atmospheric Environment, 44(33), 4116-4125. https://doi.org/10.1016/j.atmosenv.2009.05.027
- Chen, T. (2024). Los Angeles VCP study dataset. figshare. https://doi.org/10.6084/m9.figshare.25562148.v1
- Coggon, M. M., Gkatzelis, G. I., McDonald, B. C., Gilman, J. B., Schwantes, R. H., Abuhassan, N., et al. (2021). Volatile chemical product emissions enhance ozone and modulate urban chemistry. Proceedings of the National Academy of Sciences, 118(32), e2026653118. https://doi. org/10.1073/pnas.2026653118
- Czader, B. H., Li, X., & Rappenglueck, B. (2013). CMAQ modeling and analysis of radicals, radical precursors, and chemical transformations. Journal of Geophysical Research: Atmospheres, 118(19), 11376–11387. https://doi.org/10.1002/jgrd.50807
- de Gouw, J. (2021). In the footsteps of my countrymen: Atmospheric chemistry in new England, Los Angeles, and the southeast United States. Perspectives of Earth and Space Scientists, 2(1), e2021CN000151. https://doi.org/10.1029/2021CN000151
- de Gouw, J. A., Gilman, J. B., Kim, S.-W., Alvarez, S. L., Dusanter, S., Graus, M., et al. (2018). Chemistry of volatile organic compounds in the Los Angeles basin: Formation of oxygenated compounds and determination of emission ratios. Journal of Geophysical Research: Atmospheres, 123(4), 2298-2319. https://doi.org/10.1002/2017JD027976
- de Gouw, J. A., Gilman, J. B., Kim, S.-W., Lerner, B. M., Isaacman-VanWertz, G., McDonald, B. C., et al. (2017). Chemistry of volatile organic compounds in the Los Angeles basin: Nighttime removal of alkenes and determination of emission ratios. Journal of Geophysical Research: Atmospheres, 122(21), 11843-11861. https://doi.org/10.1002/2017JD027459
- Demetillo, M. A. G., Anderson, J. F., Geddes, J. A., Yang, X., Najacht, E. Y., Herrera, S. A., et al. (2019). Observing severe drought influences on ozone air pollution in California. Environmental Science and Technology, 53(9), 4695-4706. https://doi.org/10.1021/acs.est.8b04852
- Dunker, A. M., Koo, B., & Yarwood, G. (2016). Ozone sensitivity to isoprene chemistry and emissions and anthropogenic emissions in central California, Atmospheric Environment, 145, 326–337, https://doi.org/10.1016/j.atmosenv.2016.09.048
- Dusanter, S., Vimal, D., & Stevens, P. S. (2008). Technical note: Measuring tropospheric OH and HO2 by laser-induced fluorescence at low pressure. A comparison of calibration techniques, Atmospheric Chemistry and Physics, 8(2), 321–340, https://doi.org/10.5194/acp-8-321-2008
- Dusanter, S., Vimal, D., Stevens, P. S., Volkamer, R., Molina, L. T., Baker, A., et al. (2009). Measurements of OH and HO₂ concentrations during the MCMA-2006 field campaign - Part 2: Model comparison and radical budget. Atmospheric Chemistry and Physics, 9(18), 6655-6675. https://doi.org/10.5194/acp-9-6655-2009
- Edwards, P. M., Brown, S. S., Roberts, J. M., Ahmadov, R., Banta, R. M., de Gouw, J. A., et al. (2014). High winter ozone pollution from carbonyl photolysis in an oil and gas basin, *Nature*, 514(7522), 351–354, https://doi.org/10.1038/nature13767
- Emmerson, K. M., Carslaw, N., Carpenter, L. J., Heard, D. E., Lee, J. D., & Pilling, M. J. (2005). Urban atmospheric chemistry during the PUMA campaign 1: Comparison of modelled OH and HO2 concentrations with measurements. Journal of Atmospheric Chemistry, 52(2), 143-164. https://doi.org/10.1007/s10874-005-1322-3
- Emmerson, K. M., Carslaw, N., Carslaw, D. C., Lee, J. D., McFiggans, G., Bloss, W. J., et al. (2007). Free radical modelling studies during the UK TORCH Campaign in Summer 2003. Atmospheric Chemistry and Physics, 7(1), 167–181. https://doi.org/10.5194/acp-7-167-2007
- Gilman, J. B., Burkhart, J. F., Lerner, B. M., Williams, E. J., Kuster, W. C., Goldan, P. D., et al. (2010). Ozone variability and halogen oxidation within the Arctic and sub-Arctic springtime boundary layer. Atmospheric Chemistry and Physics, 10(21), 10223-10236. https://doi.org/10. 5194/acp-10-10223-2010
- Gkatzelis, G. I., Coggon, M. M., McDonald, B. C., Peischl, J., Gilman, J. B., Aikin, K. C., et al. (2021). Observations confirm that volatile chemical products are a major source of petrochemical emissions in US cities. Environmental Science and Technology, 55(8), 4332–4343. https://doi.org/10.1021/acs.est.0c05471
- Goliff, W. S., Stockwell, W. R., & Lawson, C. V. (2013). The regional atmospheric chemistry mechanism, version 2. Atmospheric Environment, 68, 174-185. https://doi.org/10.1016/j.atmosenv.2012.11.038
- Griffith, S. M., Hansen, R. F., Dusanter, S., Michoud, V., Gilman, J. B., Kuster, W. C., et al. (2016). Measurements of hydroxyl and hydroperoxy radicals during CalNex-LA: Model comparisons and radical budgets. Journal of Geophysical Research: Atmospheres, 121(8), 4211-4232.
- Hansen, R. F., Griffith, S. M., Dusanter, S., Gilman, J. B., Graus, M., Kuster, W. C., et al. (2021). Measurements of total OH reactivity during CalNex-LA. Journal of Geophysical Research: Atmospheres, 126(11), e2020JD032988. https://doi.org/10.1029/2020JD032988
- Jenkin, M. E., Saunders, S. M., Wagner, V., & Pilling, M. J. (2003). Protocol for the development of the master chemical mechanism, MCM v3 (Part B): Tropospheric degradation of aromatic volatile organic compounds. Atmospheric Chemistry and Physics, 3(1), 181–193. https://doi.

CHEN ET AL. 17 of 19

- Jiang, Z., McDonald, B. C., Worden, H., Worden, J. R., Miyazaki, K., Qu, Z., et al. (2018). Unexpected slowdown of US pollutant emission reduction in the past decade. *Proceedings of the National Academy of Sciences*, 115(20), 5099–5104. https://doi.org/10.1073/pnas.1801191115
- Kanaya, Y., Cao, R., Akimoto, H., Fukuda, M., Komazaki, Y., Yokouchi, Y., et al. (2007). Urban photochemistry in central Tokyo: 1. Observed and modeled OH and HO₂ radical concentrations during the winter and summer of 2004. *Journal of Geophysical Research*, 112(D21). https://doi.org/10.1029/2007JD008670
- Karl, T., Striednig, M., Graus, M., Hammerle, A., & Wohlfahrt, G. (2018). Urban flux measurements reveal a large pool of oxygenated volatile organic compound emissions. Proceedings of the National Academy of Sciences, 115(6), 1186–1191. https://doi.org/10.1073/pnas.1714715115
- Kim, S.-W., McDonald, B. C., Baidar, S., Brown, S. S., Dube, B., Ferrare, R. A., et al. (2016). Modeling the weekly cycle of NO_X and CO emissions and their impacts on O₃ in the Los Angeles-South Coast Air Basin during the CalNex 2010 field campaign. *Journal of Geophysical Research: Atmospheres*, 121(3), 1340–1360. https://doi.org/10.1002/2015JD024292
- Kim, S. W., McDonald, B. C., Seo, S., Kim, K. M., & Trainer, M. (2022). Understanding the paths of surface ozone abatement in the Los Angeles basin. Journal of Geophysical Research: Atmospheres, 127(4), e2021JD035606. https://doi.org/10.1029/2021JD035606
- Langford, A. O., Brioude, J., Cooper, O. R., Senff, C. J., Alvarez II, R. J., Hardesty, R. M., et al. (2012). Stratospheric influence on surface ozone in the Los Angeles area during late spring and early summer of 2010. *Journal of Geophysical Research*, 117(D21). https://doi.org/10.1029/ 2011JD016766
- Laughner, J. L., & Cohen, R. C. (2019). Direct observation of changing NO_X lifetime in North American cities. *Science*, 366(6466), 723–727. https://doi.org/10.1126/science.aax6832
- Lu, D., Tan, J., Yang, X., Sun, X., Liu, Q., & Jiang, G. (2019). Unraveling the role of silicon in atmospheric aerosol secondary formation: A new conservative tracer for aerosol chemistry. Atmospheric Chemistry and Physics, 19(5), 2861–2870. https://doi.org/10.5194/acp-19-2861-2019
- Lu, R., & Turco, R. P. (1994). Air pollutant transport in a coastal environment. Part I: Two-dimensional simulations of sea-breeze and mountain effects. *Journal of the Atmospheric Sciences*, 51(15), 2285–2308. https://doi.org/10.1175/1520-0469(1994)051<2285:APTIAC>2.0.CO;2
- Luecken, D. J., Yarwood, G., & Hutzell, W. T. (2019). Multipollutant modeling of ozone, reactive nitrogen and HAPs across the continental US with CMAQ-CB6. Atmospheric Environment, 201, 62–72. https://doi.org/10.1016/j.atmosenv.2018.11.060
- Lyu, X. P., Chen, N., Guo, H., Zhang, W. H., Wang, N., Wang, Y., & Liu, M. (2016). Ambient volatile organic compounds and their effect on ozone production in Wuhan, central China. Science of the Total Environment, 541, 200–209. https://doi.org/10.1016/j.scitotenv.2015.09.093
- McDonald, B. C., de Gouw, J. A., Gilman, J. B., Jathar, S. H., Akherati, A., Cappa, C. D., et al. (2018). Volatile chemical products emerging as largest petrochemical source of urban organic emissions. *Science*, 359(6377), 760–764. https://doi.org/10.1126/science.aaq0524
- National Oceanic and Atmospheric Administration. (2010). CalNex 2010 LA ground site data download. Retrieved from https://csl.noaa.gov/groups/csl7/measurements/2010calnex/Ground/DataDownload
- Nussbaumer, C. M., & Cohen, R. C. (2020). The role of temperature and NO_X in ozone trends in the Los Angeles basin. Environmental Science and Technology, 54(24), 15652–15659. https://doi.org/10.1021/acs.est.0c04910
- Nussbaumer, C. M., Place, B. K., Zhu, Q., Pfannerstill, E. Y., Wooldridge, P., Schulze, B. C., et al. (2023). Measurement report: Airborne measurements of NOx fluxes over Los Angeles during the RECAP-CA 2021 campaign. Atmospheric Chemistry and Physics, 23(20), 13015–13028. https://doi.org/10.5194/acp-23-13015-2023
- Peron, A., Graus, M., Striednig, M., Lamprecht, C., Wohlfahrt, G., & Karl, T. (2024). Deciphering anthropogenic and biogenic contributions to selected NMVOC emissions in an urban area. *EGUsphere*, 1–33. https://doi.org/10.5194/egusphere-2024-79
- Pfannerstill, E. Y., Arata, C., Zhu, Q., Schulze, B. C., Woods, R., Harkins, C., et al. (2023). Comparison between spatially resolved airborne flux measurements and emission inventories of volatile organic compounds in Los Angeles. *Environmental Science and Technology*, 57(41), 15533–15545. https://doi.org/10.1021/acs.est.3c03162
- Pusede, S. E., & Cohen, R. C. (2012). On the observed response of ozone to NO_X and VOC reactivity reductions in San Joaquin Valley California 1995–present. *Atmospheric Chemistry and Physics*, 12(18), 8323–8339. https://doi.org/10.5194/acp-12-8323-2012
- Qin, M., Murphy, B. N., Isaacs, K. K., McDonald, B. C., Lu, Q., McKeen, S. A., et al. (2021). Criteria pollutant impacts of volatile chemical products informed by near-field modelling. *Nature Sustainability*, 4(2), 129–137. https://doi.org/10.1038/s41893-020-00614-1
- Rappenglück, B., Dasgupta, P. K., Leuchner, M., Li, Q., & Luke, W. (2010). Formaldehyde and its relation to CO, PAN, and SO₂ in the Houston-Galveston airshed. *Atmospheric Chemistry and Physics*, 10(5), 2413–2424. https://doi.org/10.5194/acp-10-2413-2010
- Ren, X., van Duin, D., Cazorla, M., Chen, S., Mao, J., Zhang, L., et al. (2013). Atmospheric oxidation chemistry and ozone production: Results from SHARP 2009 in Houston, Texas. *Journal of Geophysical Research: Atmospheres*, 118(11), 5770–5780. https://doi.org/10.1002/jgrd.
- Ruiz, L. H., & Yarwood, G. (2013). Interactions between organic aerosol and NOy: Influence on oxidant production. Final Report for AQRP Project (pp. 12–012).
- Saunders, S. M., Jenkin, M. E., Derwent, R. G., & Pilling, M. J. (2003). Protocol for the development of the master chemical mechanism, MCM v3 (Part A): Tropospheric degradation of non-aromatic volatile organic compounds. *Atmospheric Chemistry and Physics*, 3(1), 161–180. https://doi.org/10.5194/acp-3-161-2003
- Seltzer, K. M., Murphy, B. N., Pennington, E. A., Allen, C., Talgo, K., & Pye, H. O. T. (2021b). Volatile chemical product enhancements to criteria pollutants in the United States. *Environmental Science and Technology*, 56(11), 6905–6913. https://doi.org/10.1021/acs.est.1c04298
- Seltzer, K. M., Pennington, E., Rao, V., Murphy, B. N., Strum, M., Isaacs, K. K., & Pye, H. O. T. (2021a). Reactive organic carbon emissions from volatile chemical products. *Atmospheric Chemistry and Physics*, 21(6), 5079–5100. https://doi.org/10.5194/acp-21-5079-2021
- Shah, R. U., Coggon, M. M., Gkatzelis, G. I., McDonald, B. C., Tasoglou, A., Huber, H., et al. (2020). Urban oxidation flow reactor measurements reveal significant secondary organic aerosol contributions from volatile emissions of emerging importance. *Environmental Science and Technology*, 54(2), 714–725. https://doi.org/10.1021/acs.est.9b06531
- Sheehy, P. M., Volkamer, R., Molina, L. T., & Molina, M. J. (2010). Oxidative capacity of the Mexico City atmosphere Part 2: A RO_x radical cycling perspective. *Atmospheric Chemistry and Physics*, 10(14), 6993–7008. https://doi.org/10.5194/acp-10-6993-2010
- Shirley, T. R., Brune, W. H., Ren, X., Mao, J., Lesher, R., Cardenas, B., et al. (2006). Atmospheric oxidation in the Mexico City metropolitan area (MCMA) during april 2003. Atmospheric Chemistry and Physics, 6(9), 2753–2765. https://doi.org/10.5194/acp-6-2753-2006
- South Coast Air Quality Management District. (1997). History of air pollution control in southern California. Retrieved from https://www.aqmd.gov/home/research/publications/history-of-air-pollution-control
- Tan, Z., Lu, K., Jiang, M., Su, R., Wang, H., Lou, S., et al. (2019). Daytime atmospheric oxidation capacity in four Chinese megacities during the photochemically polluted season: A case study based on box model simulation. Atmospheric Chemistry and Physics, 19(6), 3493–3513. https://doi.org/10.5194/acp-19-3493-2019
- Wang, N., Guo, H., Jiang, F., Ling, Z. H., & Wang, T. (2015). Simulation of ozone formation at different elevations in mountainous area of Hong Kong using WRF-CMAQ model. Science of the Total Environment, 505, 939–951. https://doi.org/10.1016/j.scitotenv.2014.10.070

CHEN ET AL. 18 of 19

- Wang, T., Xue, L., Feng, Z., Dai, J., Zhang, Y., & Tan, Y. (2022). Ground-level ozone pollution in China: A synthesis of recent findings on influencing factors and impacts. *Environmental Research Letters*, 17(6), 063003. https://doi.org/10.1088/1748-9326/ac69fe
- Wang, Y., Guo, H., Zou, S., Lyu, X., Ling, Z., Cheng, H., & Zeren, Y. (2018). Surface O₃ photochemistry over the South China Sea: Application of a near-explicit chemical mechanism box model. *Environmental Pollution*, 234, 155–166. https://doi.org/10.1016/j.envpol.2017.11.001
- Wang, Y., Wang, H., Guo, H., Lyu, X., Cheng, H., Ling, Z., et al. (2017). Long-term O₃-precursor relationships in Hong Kong: Field observation and model simulation. *Atmospheric Chemistry and Physics*, 17(18), 10919–10935. https://doi.org/10.5194/acp-17-10919-2017
- Warneke, C., de Gouw, J. A., Holloway, J. S., Peischl, J., Ryerson, T. B., Atlas, E., et al. (2012). Multiyear trends in volatile organic compounds in Los Angeles, California: Five decades of decreasing emissions. *Journal of Geophysical Research*, 117(D21). https://doi.org/10.1029/2012JD017899
- Warneke, C., Veres, P., Holloway, J. S., Stutz, J., Tsai, C., Alvarez, S., et al. (2011). Airborne formaldehyde measurements using PTR-MS: Calibration, humidity dependence, inter-comparison and initial results. *Atmospheric Measurement Techniques*, 4(10), 2345–2358. https://doi.org/10.5194/amt-4-2345-2011
- Washenfelder, R. A., Young, C. J., Brown, S. S., Angevine, W. M., Atlas, E. L., Blake, D. R., et al. (2011). The glyoxal budget and its contribution to organic aerosol for Los Angeles, California, during CalNex 2010. *Journal of Geophysical Research*, 116(D21). https://doi.org/10.1029/ 2011JD016314
- Wolfe, G. M., Marvin, M. R., Roberts, S. J., Travis, K. R., & Liao, J. (2016). The framework for 0-D atmospheric modeling (F0AM) v3.1. Geoscientific Model Development, 9(9), 3309–3319. https://doi.org/10.5194/gmd-9-3309-2016
- Wu, Y., & Johnston, M. V. (2017). Aerosol Formation from OH oxidation of the volatile cyclic methyl siloxane (cVMS) decamethylcyclopentasiloxane. Environmental Science and Technology, 51(8), 4445–4451. https://doi.org/10.1021/acs.est.7b00655
- Yarwood, G., Jung, J., Whitten, G. Z., Heo, G., Mellberg, J., & Estes, M. J. (2010). Updates to the carbon bond mechanism for version 6 (CB6).
 Zhang, J., Wei, Y., & Fang, Z. (2019). Ozone pollution: A major health hazard worldwide. Frontiers in Immunology, 10. https://doi.org/10.3389/fimmu.2019.02518
- Zhang, L., Brook, J. R., & Vet, R. (2003). A revised parameterization for gaseous dry deposition in air-quality models. *Atmospheric Chemistry and Physics*, 3(6), 2067–2082. https://doi.org/10.5194/acp-3-2067-2003
- Zhu, Q., Schwantes, R. H., Coggon, M., Harkins, C., Schnell, J., He, J., et al. (2023). A better representation of VOC chemistry in WRF-Chem and its impact on ozone over Los Angeles. *EGUsphere*, 1–31. https://doi.org/10.5194/egusphere-2023-2742
- Zhu, S., Kinnon, M. M., Shaffer, B. P., Samuelsen, G. S., Brouwer, J., & Dabdub, D. (2019). An uncertainty for clean air: Air quality modeling implications of underestimating VOC emissions in urban inventories. Atmospheric Environment, 211, 256–267. https://doi.org/10.1016/j.atmosenv.2019.05.019
- Zong, R., Xue, L., Wang, T., & Wang, W. (2018). Inter-comparison of the regional atmospheric chemistry mechanism (RACM2) and master chemical mechanism (MCM) on the simulation of acetaldehyde. *Atmospheric Environment*, 186, 144–149. https://doi.org/10.1016/j.atmosenv. 2018.05.013

CHEN ET AL. 19 of 19